SIAM J. Applied Dynamical Systems
Vol. 12, No. 1, pp. 415–449

Stationary States in Infinite Networks of Spiking Oscillators with Noise*

Stilianos Louca[†‡] and Fatihcan M. Atay[†]

Abstract. We model networks of identical, all-to-all, pulse-coupled phase oscillators with white noise, in the limit of infinite network size and Dirac pulses, using a Fokker–Planck equation for the phase probability density. We give analytical, constructive existence and uniqueness results for stationary states (i.e., time-independent densities) and derive and study a one-dimensional eigenvalue equation for their linear stability. Our results are supplemented by numerical methods, which are applied to two classes of oscillator response functions. We find that the stationary network activity depends for some response functions monotonically and for others nonmonotonically on the coupling and noise strength. In all cases we find that a sufficiently strong noise locally stabilizes the stationary state, and simulations suggest this stability to be global. For most response functions the stationary state undergoes a supercritical Hopf bifurcation as noise is decreased, and a locally stable limit cycle emerges in its proximity. On that limit cycle, the network splits into groups of approximately synchronized oscillators, while the network's (mean) activity oscillates at frequencies often much higher than the intrinsic oscillator frequency.

Key words. Winfree model, coupled oscillators, Fokker–Planck equation, stationary state, noise, stability

AMS subject classifications. 47J35, 35Q84, 34C15, 47A75

DOI. 10.1137/120880264

1. Introduction.

We study networks of all-to-all, pulse-coupled, identical phase oscillators with additive white noise in the limit where the size of the network tends to infinity and the pulses tend to Dirac distributions (the so-called *spikes*). Specifically, we examine the nonlinear *Fokker–Planck equation* [17]

$$\partial_t \rho(t,\vartheta) = -\partial_\vartheta \Big[\rho(t,\vartheta) \cdot [\omega + \psi(\vartheta)\rho(t,0)] \Big] + D\partial_\vartheta^2 \rho(t,\vartheta) \tag{1.1}$$

in the time-dependent probability density $\rho(t,\vartheta)$ for oscillator phases $\vartheta \in S^1 \cong \mathbb{R}/\mathbb{Z}$, where $\psi : S^1 \to \mathbb{R}$. Here, $\omega > 0$ is the intrinsic oscillator frequency and $D \geq 0$ the diffusion coefficient as a measure for the intensity of the noise which each oscillator is subject to. Equation (1.1) can be seen as a limit of the Fokker–Planck equation

$$\partial_t \rho(t,\vartheta) = -\partial_\vartheta \left[\rho(t,\vartheta) \cdot \left[\omega + \psi(\vartheta) \int_{S^1} d\varphi \; \rho(t,\varphi) P(\varphi) \right] \right] + D\partial_\vartheta^2 \rho(t,\vartheta) \tag{1.2}$$

as the *pulse* $P : S^1 \to \mathbb{R}_+$ tends to the Dirac distribution at phase zero, the so-called *firing point*. The noise-free version of (1.2) has been extensively used as a thermodynamic limit (i.e.,

*Received by the editors June 8, 2012; accepted for publication (in revised form) by B. Ermentrout December 20, 2012; published electronically March 12, 2013. This work was supported by the Max Planck Society.
http://www.siam.org/journals/siads/12-1/88026.html
[†]Max Planck Institute for Mathematics in the Sciences, Inselstraße 22, 04103 Leipzig, Germany (Stilianos.Louca@gmail.com, fatay@mis.mpg.de).
[‡]Current address: Institute of Applied Mathematics, University of British Columbia, Vancouver, B.C. V6T 1Z2, Canada.

as $N \to \infty$) of the Winfree model [6, 52]

$$\frac{d\theta_i(t)}{dt} = \omega + \frac{\psi(\theta_i)}{N} \sum_{j=1}^{N} P(\theta_j), \qquad i = 1, \ldots, N, \tag{1.3}$$

for N all-to-all pulse-coupled phase oscillators with phases θ_i [5, 6, 7, 20], which was originally introduced in [52] for the modeling of interacting biological oscillators that are coupled so weakly that after any coupling-induced perturbation they return to their attractor, albeit with a certain phase shift. The *response function* (or *response*, for short) ψ mediates the influence of the stimulus $N^{-1} \sum_j P(\theta_j)$ on the phase of the oscillators and can be seen as a direct analogue of the infinitesimal phase response curve used in neural network theory [22, 15, 45]. Reference [26, sects. 3.2 and 5.2] gives a derivation of such dynamics using a perturbation analysis around stable limit cycles, where the authors assume a short stimulus distorting the oscillator dynamics as an additive term in the full equations of motion. We note that it is not always clear what form such a stimulus should have, as a result of overall network activity. The *mean field* form, used for the stimulus in (1.3), is justified by the assumption of weak interactions and is thus an additive effect of simultaneous perturbations.

The density $\rho(t, \cdot)$ in (1.2) has two interpretations. On one hand, it can be seen as the probability density of oscillator phases on S^1 as their number grows to infinity. On the other hand, it is the probability density of a stochastic process $\hat{\theta}$ satisfying the Langevin equation [41, sect. 4.4]

$$d\hat{\theta}(t) = \Big[\omega + \psi(\hat{\theta}(t))S(t)\Big]\, dt + \sqrt{2D} dW(t),$$

with W as a Wiener process and $S(t) := \int_{S^1} d\varphi\ \rho(t, \varphi)P(\varphi)$ as a time-dependent *stimulus*. Drawing upon the equivalence of oscillators in the finite Winfree model, we shall identify the network state with the single probability density $\rho(t, \cdot)$. Note that behind such a mean field description lies the assumption that the oscillator states are identically and independently distributed at all times, provided they are so initially. It has recently been shown that this so-called *propagation of chaos* [24, 13] is satisfied for even more general networks in the limit as $N \to \infty$ [48]. Continuum models similar to (1.2) have been considered in the past for the famous Kuramoto model of coupled phase oscillators [26, 42, 47, 46, 2]. The propagation of chaos in the Kuramoto model is well established [9, 10, 2].

The approximation of oscillator pulses P by Dirac distributions may be particularly meaningful for certain neuronal oscillators, as action potentials of periodically firing neurons can be of significantly shorter duration than the firing periods themselves. For example, the inhalation of odor molecules has been found to trigger oscillations of the local field potential of mitral cells in the olfactory bulb of rats, within the frequency range 20–80 Hz and with spikes lasting just about 2 ms [14, 27]. Note that to arrive at (1.1), the limit of Dirac pulses is taken *after* the limit of an infinite network size. The case where oscillator phases in finite networks discontinuously jump due to other spiking oscillators has been extensively studied in the literature (see, for example, [21] and the references therein). By taking the limit of Dirac pulses after the limit $N \to \infty$, one obtains a well-behaved partial differential equation instead of a discontinuous ordinary one.

1.1. Overview. We study the existence, uniqueness, and local as well as global stability of *stationary probability densities*, that is, time-independent solutions to the Fokker–Planck equation (1.1). As it turns out, the local dynamics related to these stationary states are strongly linked to the attractors and long term dynamics of the network. In view of possible applications to neural networks, special interest is devoted to the network stimulus (or *activity*) $\rho(t,0)$. The latter can be seen as an analogue of the synaptic or firing rate activity in populations of neurons. We study its time evolution and its dependence on the network parameters in case of stationarity. Throughout the paper the main parameters of interest will be the so-called *coupling strength* $\|\psi\|_\infty/\omega$ and *noise strength* D/ω. Our analytical findings are supplemented by numerical results.

In section 2 we give existence and uniqueness results for stationary states in networks with responses $\psi \in \mathcal{C}^2(S^1,\mathbb{R})$. Throughout, we shall mainly for simplicity assume $\psi(0)=0$, though most of our analytical results can be extended to more general responses. Many response functions derived from biophysical neuron models or determined through experiments on real neurons satisfy this assumption (see [15, 34, 40] for examples). We show that determining stationary states is equivalent to solving certain one-dimensional fixed point equations. These *stationary state equations* are integral equations in the stationary stimulus and are derived using a self-consistency argument. Furthermore, we look at the transition of stationary states in the limits $D\to 0$ and $D\to\infty$.

In section 3 we perform a local stability analysis of stationarity. For the noise-free case, we derive a one-dimensional integral eigenvalue equation for the linear dynamics at stationary states.

In section 4 we present numerical methods for the evaluation of the stationary state equations and the spectral stability analysis of stationary states in noise-free as well as noisy networks. We furthermore present an explicit numerical integration scheme for the Fokker–Planck equation (1.1) based on a spectral method introduced by [36] for the Kuramoto model. Many technical details of the numerical analysis are given in Appendix B.

We then apply our analytical results and numerical methods to two concrete response families, namely, *type* I *responses* of the form

$$\psi(\vartheta) = \frac{\psi_o}{2}\left[1-\cos\left(2\pi\cdot\xi(\vartheta;\vartheta_o)\right)\right] \tag{1.4}$$

and *type* II *responses* of the form

$$\psi(\vartheta) = -\psi_o \sin(2\pi\cdot\xi(\vartheta;\vartheta_o)), \tag{1.5}$$

where

$$\xi(\vartheta;\vartheta_o) := \vartheta + \frac{1}{2}(1-2\vartheta_o)\,\frac{1-\cos\left(2\pi\vartheta\right)}{1-\cos\left(2\pi\vartheta_o\right)}.$$

The *amplitude* ψ_0 and the *turning point* $\vartheta_o\in(0,1)$ are parameters of the response functions. We call the response *symmetric* if $\vartheta_o = 0.5$. See Figure 1.

The two-type classification of responses follows the ideas of [15] and [22], who linked the type of phase response curves [45] to the bifurcation types of excitable neuron membranes.

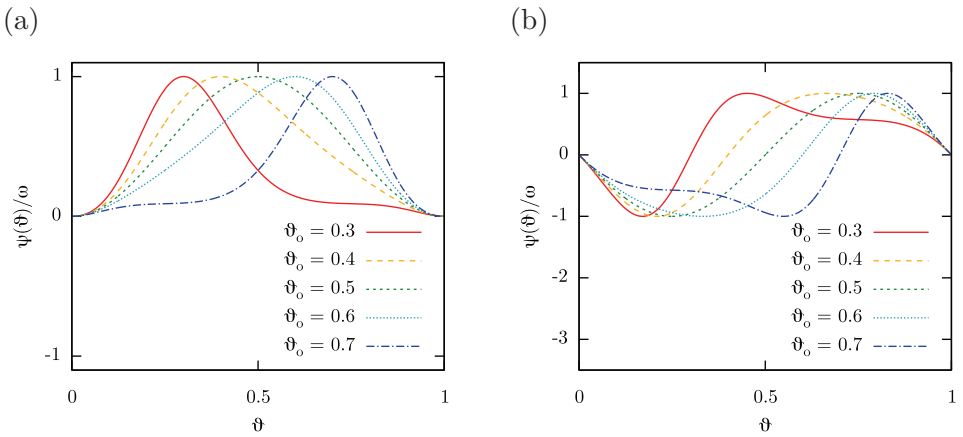

Figure 1. *Illustration of accelerating type* I (a) *and attracting type* II (b) *responses for* $\psi_o/\omega = 1$. *Note that for type* I *responses with* $\vartheta_o \approx 0.5$, ϑ_o *corresponds to the local extremum other than the origin, whereas for type* II *responses it corresponds to the point of sign change other than the origin.*

We shall call a type I response *accelerating* or *delaying* if $\psi_o > 0$ or $\psi_o < 0$, respectively. We shall call a type II response *attracting* or *repulsing* if $\psi_o > 0$ or $\psi_o < 0$, respectively, due to the way oscillators near the firing point react to incoming stimuli from other, firing oscillators. We chose to study these two response families because they generalize their symmetric versions, which have already drawn attention in the literature (see [5] and [15, eq. (2.8)]). Furthermore, they qualitatively resemble several infinitesimal phase response curves measured on real neurons [33, 34, 40].

Type I and type II responses are considered in sections 5 and 6, respectively. We show how stationary states and their stability vary with the response parameters and the noise strength. We restrict our attention to the ranges $\vartheta_o \in [0.3, 0.7]$, $|\psi_o|/\omega \in [0, 0.5]$, and $D/\omega \in [0, 1]$. Our linear stability analysis shows that, for almost all responses, stationarity is unstable for sufficiently weak noise. In that realm, numerical integration of the Fokker–Planck equation (1.1) reveals the existence of a stable limit cycle, on which the network splits into multiple groups of approximately synchronized oscillators. By *synchrony* we mean the persistence of a common time-dependent phase among oscillators within each group. The number of groups equals, at least in most of the cases, the order of the leading eigenperturbation of stationarity. The limit cycle, the stationary state, and the orbits connecting the two constitute an attractor of the system. Above a certain noise threshold the limit cycle merges with the stationary state, which then becomes locally stable and, apparently, also globally stable. We note that contrary to the better understood Kuramoto model, the dynamics studied here are not rotational invariant, which makes the analytical description of nontrivial invariant manifolds somewhat more difficult. Particularly, the ansatz of Ott and Antonsen [35] for a low dimensional solution fails to work.

We finish with a short comparison of the predictions of the Fokker–Planck equation (1.1) to the finite Winfree model (1.3) with continuous pulses $P \in \mathcal{C}(S^1, \mathbb{R}_+)$ and additive white

noise. For that purpose we numerically integrate the Langevin equation

$$d\hat{\theta}_i(t) = \left[\omega + \psi(\hat{\theta}_i(t))\frac{1}{N}\sum_{j=1}^{N} P(\hat{\theta}_j(t))\right]dt + \sqrt{2D}dW_i(t) \tag{1.6}$$

for the stochastic processes $\hat{\theta}_1, \ldots, \hat{\theta}_N$ on S^1, with $W_1, \ldots, W_N$ being independent Wiener processes. We consider both type I and type II responses. We are particularly interested in a comparison of the long term network behavior in the two models for large N and narrow pulses P (with $\int_{S^1} d\varphi\ P(\varphi) = 1$). The results are presented in section 7 and indicate a good agreement of the two models for large N and small pulse widths. We mention that similar comparisons have been made in the past for the Kuramoto model and have also shown a strong agreement between finite networks and their thermodynamic limit for sufficiently large N [37, 12, 23].

1.2. Notation. We denote $\mathbb{R}_+ := [0, \infty)$ and $\mathbb{N}_0 := \mathbb{N} \cup \{0\}$. For any smooth manifold M we write $\mathcal{C}^k(M, \mathbb{R}_+)$ for the class of k-times continuously differentiable functions mapping M to $\mathbb{R}_+$. We denote by $\|\cdot\|_\infty$ the supremum norm. For $h \in \mathcal{C}(S^1, \mathbb{C})$, we denote by $\mathcal{F}_n(h) := \int_{S^1} d\varphi\, h(\varphi) \cdot e^{-in2\pi\cdot\varphi}$ its nth Fourier component, $n \in \mathbb{Z}$. By $\mathcal{C}^k_{\mathrm{zm}}(S^1)$ we denote the class of complex-valued $\mathcal{C}^k$ functions on S^1 with zero mean; that is,

$$\mathcal{C}^k_{\mathrm{zm}}(S^1) := \left\{ f \in \mathcal{C}^k(S^1, \mathbb{C}) : \int_{S^1} d\varphi\ f(\varphi) = 0 \right\}.$$

For $\lambda \in \mathbb{C}$ we write λ^* for its complex conjugate. Let $\Pi_c : \mathbb{R} \to S^1 = \mathbb{R}/\mathbb{Z}$ be the canonical projection of reals to angles. For $f : S^1 \to \mathbb{C}$ and $\vartheta \in \mathbb{R}$, we will abbreviate $f(\Pi_c(\vartheta))$ as $f(\vartheta)$ whenever the meaning is clear from the context.

2. Existence and uniqueness of stationary states.

In this section we present analytical results for the existence and uniqueness of stationary states. We assume $\omega > 0$, $\psi \in \mathcal{C}^2(S^1, \mathbb{R})$, $\psi(0) = 0$, and $D \geq 0$.

2.1. Existence and uniqueness in noise-free networks. In the noise-free case ($D = 0$), stationary probability densities $\rho_s \in \mathcal{C}^1(S^1, \mathbb{R}_+)$ are nonnegative normalized L^1 solutions to the differential equation

$$\frac{d}{d\vartheta}\Big[\rho_s(\vartheta) \cdot [\omega + \psi(\vartheta)\rho_s(0)]\Big] = 0. \tag{2.1}$$

Condition (2.1) can be interpreted as the *probability flux* $\rho_s(\vartheta)\cdot[\omega + \psi(\vartheta) \cdot \rho_s(0)]$ being constant on S^1. Since $\psi(0) = 0$, the flux must be strictly positive. This yields the form

$$\rho_s(\vartheta) = \frac{\omega\rho_s(0)}{\omega + \psi(\vartheta)\rho_s(0)} \tag{2.2}$$

for all stationary densities ρ_s. The condition that ρ_s be a probability density translates to the fixed-point equation

$$\rho_s(0) = \frac{1}{\omega}\left[\int_{S^1} \frac{d\vartheta}{\omega + \psi(\vartheta)\rho_s(0)}\right]^{-1} \tag{2.3}$$

in the stationary stimulus $\rho_s(0) > 0$. Conversely, solving (2.3) (under the condition $\omega + \psi(\vartheta)\rho_s(0) > 0$ for all $\vartheta \in S^1$) yields through (2.2) a stationary probability density. We shall refer to (2.3) as the *stationary state equation* for noise-free networks. The following lemma gives a sufficient condition for the existence and uniqueness of its solutions.

Lemma 2.1. *Suppose the coupling strength* $\mathcal{E} := \|\psi\|_\infty / \omega$ *is strictly smaller than* $\frac{1}{2}$. *Then there exists a unique stationary probability density* $\rho_s \in \mathcal{C}^1(S^1, \mathbb{R})$. *The stationary stimulus* $\rho_s(0)$ *is within* $(2/3, 2)$. *Moreover,* $\rho_s \to 1$ *uniformly as* $\mathcal{E} \to 0$.

Proof. Abbreviating the right-hand side of (2.3) by $A_0(\rho_s(0))$, for any stationary probability density ρ_s one can easily estimate

$$A_0(\rho_s(0)) \leq 1 + \mathcal{E}\rho_s(0), \tag{2.4}$$

which, by (2.3) and $\mathcal{E} < \frac{1}{2}$, implies that $\rho_s(0) < 2$. Note that $A_0(r)$ is well defined for $r \in [0, 2]$ and that the compact interval $J := [0, 2]$ is A_0-invariant. The function $A_0 : J \to J$ is continuous and differentiable on $J^o := (0, 2)$, with derivative

$$A_0'(r) = \frac{A_0^2(r)}{\omega} \int_{S^1} \frac{\psi(\vartheta)\, d\vartheta}{\left[1 + \frac{r}{\omega}\psi(\vartheta)\right]^2}. \tag{2.5}$$

Since the mapping $x \mapsto \frac{x}{1+\alpha x}$ (where $\alpha \geq 0$) is increasing in x for $x > -1/\alpha$, one has

$$\frac{\psi(\vartheta)}{[1 + \alpha\psi(\vartheta)]^2} \leq \frac{\psi(\vartheta)}{1 + \alpha\psi(\vartheta)} \leq \frac{\|\psi\|_\infty}{1 + \alpha \|\psi\|_\infty} \tag{2.6}$$

whenever $\psi(\vartheta) > -1/\alpha$. Letting $\alpha := r/\omega$ for any $r \in (0, 2)$ leads by (2.5) and (2.6) to the estimate

$$A_0'(r) \leq \frac{\mathcal{E} A_0^2(r)}{1 + \mathcal{E}r} \leq \frac{\mathcal{E}\,[1 + \mathcal{E}r]^2}{1 + \mathcal{E}r} \leq \mathcal{E}\,[1 + 2\mathcal{E}] < 1$$

for all $r \in (0, 2)$. Therefore, $A_0 : J \to J$ has a unique fixed point r_o. It corresponds to a stationary probability density ρ_s with $\rho_s(0) = r_o$ having the form (2.2). Similarly to (2.4), one can also estimate $A_0(\rho_s(0)) \geq 1 - \mathcal{E}\rho_s(0)$, which implies $\rho_s(0) > 2/3$. In fact, together with (2.4) this implies

$$\frac{1}{1 + \mathcal{E}} \leq \rho_s(0) \leq \frac{1}{1 - \mathcal{E}},$$

which shows that $\rho_s(0) \to 1$ as $\mathcal{E} \to 0$. Thus by (2.3), $\rho_s \to 1$ uniformly as $\mathcal{E} \to 0$. ∎

2.2. Existence and local uniqueness in networks with noise. In the case $D > 0$, stationary states $\rho_s \in \mathcal{C}^2(S^1, \mathbb{R}_+)$ are nonnegative normalized L^1 solutions to the differential equation

$$\frac{d}{d\vartheta}\Big[\rho_s(\vartheta) \cdot [\omega + \psi(\vartheta)\rho_s(0)] - D\frac{d}{d\vartheta}\rho_s(\vartheta)\Big] = 0.$$

This is equivalent to

$$\frac{d}{d\vartheta}\rho_s(\vartheta) = \frac{1}{D}\,[\omega + \psi(\vartheta)\rho_s(0)]\,\rho_s(\vartheta) + C \tag{2.7}$$

for some appropriate constant $C \in \mathbb{R}$. For fixed stimulus $\rho_s(0)$, (2.7) is a first-order ODE, admitting on $[0,1]$ the unique solution

$$\rho_s(\vartheta) = \exp\left[\frac{1}{D}\left[\omega\vartheta + \Psi(0,\vartheta)\rho_s(0)\right]\right] \cdot \left[C\int_0^\vartheta d\varphi\ \exp\left[-\frac{1}{D}\left[\omega\varphi + \Psi(0,\varphi)\rho_s(0)\right]\right] + \rho_s(0)\right],$$

where $\Psi(\vartheta_1,\vartheta_2) := \int_{\vartheta_1}^{\vartheta_2} d\varphi\ \psi(\varphi)$. The periodicity condition $\rho_s(0) = \rho_s(1)$ determines the constant C and eventually leads to the representation

$$\begin{aligned}\rho_s(\vartheta) = \rho_s(0)&\left\{\int_0^1 d\varphi\ \exp\left[-\frac{1}{D}\left[\omega\varphi + \Psi(0,\varphi)\rho_s(0)\right]\right]\right\}^{-1}\\ &\times\int_0^1 d\varphi\ \exp\left[-\frac{1}{D}\left[\omega\varphi + \Psi(\vartheta,\vartheta+\varphi)\rho_s(0)\right]\right],\end{aligned} \tag{2.8}$$

where we used the fact that $\Psi(0,1) + \Psi(0,\varphi) = \Psi(0,1+\varphi)$. Finally, the normalization condition $\int_0^1 d\vartheta\ \rho_s(\vartheta) = 1$ is equivalent to the fixed-point equation

$$\begin{aligned}\rho_s(0) = &\left\{\int_0^1 d\vartheta\ \int_0^1 d\varphi\ \exp\left[-\frac{1}{D}\left[\omega\varphi + \Psi(\vartheta,\vartheta+\varphi)\rho_s(0)\right]\right]\right\}^{-1}\\ &\times\int_0^1 d\varphi\ \exp\left[-\frac{1}{D}\left[\omega\varphi + \Psi(0,\varphi)\rho_s(0)\right]\right]\end{aligned} \tag{2.9}$$

in the stationary stimulus $\rho_s(0) > 0$. Conversely, the solutions to (2.9) correspond through (2.8) to stationary probability densities, which by (2.7) are of class $\mathcal{C}^2(S^1,\mathbb{R}_+)$. Similarly to (2.3), we refer to (2.9) as the *stationary state equation* for networks with noise. The following results provide existence and local uniqueness statements for the solutions.

Proposition 2.2. *Let $A_D(\rho_s(0))$ denote the right-hand side of (2.9), and denote $J_\beta = [0,\beta]$. Suppose $\beta \geq 2$ and $\mathcal{E} := \|\psi\|_\infty/\omega \leq 1/(4\beta)$. Then $A_D(J_\beta) \subseteq J_{5/3}$, and the mapping $A_D : J_\beta \to J_{5/3}$ is a contraction with a Lipschitz constant not depending on D or β.*

Proof. We define two auxiliary functions $\zeta,\eta : \mathbb{R} \to \mathbb{R}_+$ by

$$\begin{aligned}\zeta(s) &:= \int_0^1 d\varphi\ e^{-s\varphi} = \frac{1}{s}\left[1 - e^{-s}\right],\\ \eta(s) &:= \int_0^1 d\varphi\ e^{-s\varphi}\varphi = \frac{1}{s^2}\left[1 - e^{-s} - se^{-s}\right].\end{aligned} \tag{2.10}$$

(The values at $s = 0$ are equal to 1 and $\frac{1}{2}$, respectively, from the integrals.) Note that for $0 \leq s_1 \leq s_2$,

$$\frac{\zeta(s_1)}{\zeta(s_2)} \leq \frac{s_2}{s_1}, \qquad \frac{\eta(s_1)}{\zeta(s_2)} \leq \frac{s_2}{s_1^2}. \tag{2.11}$$

Let $M(\rho_s(0))$ and $N(\rho_s(0))$ denote the numerator and denominator on the right-hand side of (2.9), respectively, so that $A_D = M/N$. For $r, r_1, r_2 \geq 0$, it is straightforward to obtain the

estimates

$$
\begin{aligned}
&|M(r)| \leq \zeta\left[\frac{\omega}{D}(1-\mathcal{E}r)\right],\\
&\zeta\left[\frac{\omega}{D}(1+\mathcal{E}r)\right] \leq |N(r)| \leq \zeta\left[\frac{\omega}{D}(1-\mathcal{E}r)\right],\\
&|M(r_1)-M(r_2)| \leq \frac{\|\psi\|_\infty}{D}\cdot\eta\left[\frac{\omega}{D}\left[1-\mathcal{E}\max(r_1,r_2)\right]\right]\cdot|r_1-r_2|,\\
&|N(r_1)-N(r_2)| \leq \frac{\|\psi\|_\infty}{D}\cdot\eta\left[\frac{\omega}{D}\left[1-\mathcal{E}\max(r_1,r_2)\right]\right]\cdot|r_1-r_2|.
\end{aligned}
$$

Combining them leads to the estimate

$$
|A_D(r)| \leq \frac{\zeta\left[\frac{\omega}{D}(1-\mathcal{E}r)\right]}{\zeta\left[\frac{\omega}{D}(1+\mathcal{E}r)\right]} \tag{2.12}
$$

and (assuming $r_1 \geq r_2$) to

$$
\begin{aligned}
|A_D(r_1)-A_D(r_2)| &\leq \frac{\left[\,|N(r_2)|\cdot|M(r_1)-M(r_2)|+|N(r_1)-N(r_2)|\cdot|M(r_2)|\,\right]}{|N(r_1)N(r_2)|}\\
&\leq 2\mathcal{E}\cdot\frac{\eta\left[\frac{\omega}{D}(1-\mathcal{E}r_1)\right]\zeta\left[\frac{\omega}{D}(1-\mathcal{E}r_2)\right]}{\zeta\left[\frac{\omega}{D}(1+\mathcal{E}r_1)\right]\zeta\left[\frac{\omega}{D}(1+\mathcal{E}r_2)\right]}\cdot\frac{\omega}{D}|r_1-r_2|.
\end{aligned} \tag{2.13}
$$

Now let $\beta \geq 2$, and assume $\mathcal{E} \leq 1/(4\beta)$. Then $\mathcal{E}r < 1$ for all $r \in J_\beta$. By applying (2.11) to (2.12) we find that

$$
|A_D(r)| \leq \frac{1+\mathcal{E}r}{1-\mathcal{E}r} \leq \frac{1+\mathcal{E}\beta}{1-\mathcal{E}\beta} \leq \frac{5}{3}
$$

for all $r \in J_\beta$, so that indeed $A_D(J_\beta) \subseteq J_{5/3}$. Similarly, by applying (2.11) to (2.13), we find

$$
\begin{aligned}
|A_D(r_1)-A_D(r_2)| &\leq 2\mathcal{E}\cdot\frac{1+\mathcal{E}r_1}{(1-\mathcal{E}r_1)^2}\cdot\frac{1+\mathcal{E}r_2}{1-\mathcal{E}r_2}\cdot|r_1-r_2|\\
&\leq \frac{1}{2\beta}\cdot\frac{(1+\mathcal{E}\beta)^2}{(1-\mathcal{E}\beta)^3}\cdot|r_1-r_2| \leq \frac{25}{27}|r_1-r_2|
\end{aligned}
$$

for all $r_1, r_2 \in J_\beta$. ∎

Proposition 2.3. *For $D > 0$, let $A_0, A_D : \mathbb{R}_+ \to \mathbb{R}_+$ be the functionals introduced in Lemma 2.1 and Proposition 2.2, respectively. Let $\mathcal{E} := \|\psi\|_\infty/\omega$ and $r \geq 0$ be such that $\mathcal{E}r < 1$. Then $A_D(r)$ tends to $A_0(r)$ as $D \to 0^+$.*

Proof. The proof is based on the following easily verifiable fact: If $f \in \mathcal{C}([0,1],\mathbb{R})$ is (right-)differentiable at 0 with $f'(0) > 0$, and 0 is the unique global minimum of f, then

$$
\lim_{D\to 0^+}\left\{\int_0^1 d\varphi\ \exp\left[-\frac{1}{D}f(\varphi)\right]\right\}^{-1}\cdot\int_0^1 d\varphi\ \exp\left[-\frac{1}{D}\left[f(0)+f'(0)\varphi\right]\right] = 1. \tag{2.14}
$$

For each $\vartheta \in [0,1]$ consider the function $f_\vartheta : [0,1] \to \mathbb{R}$ defined as $f_\vartheta(\varphi) := \omega\varphi + \Psi(\vartheta, \vartheta+\varphi)r$. Then f_ϑ satisfies the assumptions of the above assertion with $f'_\vartheta(0) = \omega + \psi(\vartheta)r > 0$. By (2.14) this implies that

$$\begin{aligned}\lim_{D\to 0^+} A_D(r) &= \left\{ \int_0^1 d\vartheta \ \lim_{D\to 0^+} \left[\int_0^1 d\varphi \ \exp\left[-\frac{1}{D}\left[\omega + \psi(0)r\right]\varphi \right] \right]^{-1} \right. \\ &\qquad \left. \times \int_0^1 d\varphi \ \exp\left[-\frac{1}{D}\left[\omega + \psi(\vartheta)r\right]\varphi \right] \right\}^{-1} \\ &= \left\{ \int_0^1 d\vartheta \ \lim_{D\to 0^+} \zeta\left[\frac{\omega}{D}\right]^{-1} \zeta\left[\frac{1}{D}\left[\omega + \psi(\vartheta)r\right]\right] \right\}^{-1} \\ &= \left[\omega \int_0^1 \frac{d\vartheta}{\omega + \psi(\vartheta)r} \right]^{-1} = A_0(r),\end{aligned}$$

with $\zeta : \mathbb{R}_+ \to \mathbb{R}_+$ being the auxiliary function introduced in (2.10), where we used Lebesgue's dominated convergence theorem to swap the limit with the ϑ-integral. The latter holds due to the estimate

$$\begin{aligned}&\left\{ \int_0^1 d\varphi \ \exp\left[-\frac{1}{D}\left[\omega\varphi + \Psi(0,\varphi)r\right]\right] \right\}^{-1} \int_0^1 d\varphi \ \exp\left[-\frac{1}{D}\left[\omega\varphi + \Psi(\vartheta,\vartheta+\varphi)r\right]\right] \\ &\leq \left\{ \int_0^1 d\varphi \ \exp\left[-\frac{1}{D}\left[\omega + \|\psi\|_\infty r\right]\varphi \right] \right\}^{-1} \int_0^1 d\varphi \ \exp\left[-\frac{1}{D}\left[\omega - \|\psi\|_\infty r\right]\varphi \right] \\ &= \frac{\zeta\left[\frac{\omega}{D}\left[1 - \mathcal{E}r\right]\right]}{\zeta\left[\frac{\omega}{D}\left[1 + \mathcal{E}r\right]\right]} < \infty\end{aligned}$$

holding uniformly in ϑ. ∎

Lemma 2.4. *Let $\beta \geq 2$ and $\mathcal{E} = \|\psi\|_\infty / \omega \leq 1/(4\beta)$. Then for every $D > 0$ there exists exactly one stationary probability density $\rho_s \in \mathcal{C}^2(S^1, \mathbb{R})$ such that $\rho_s(0) \in J_\beta := [0, \beta]$. The density ρ_s in fact satisfies $\rho_s(0) \in [0, 5/3]$. As $D \to 0^+$, ρ_s converges pointwise to the stationary probability density for noise-free networks (the existence and uniqueness of which are ensured by Lemma 2.1). Furthermore, the density ρ_s depends continuously (in the supremum norm) on $D > 0$.*

Proof. By Proposition 2.2, the functionals $A_D : J_\beta \to J_{5/3} \subseteq J_\beta$ $(D > 0)$ are contractions with a Lipschitz constant $L_A < 1$ not depending on D. By Banach's fixed-point theorem, each A_D has a unique fixed-point r_D in J_β corresponding to the stationary state $\rho_s(\cdot\,; D, r_D)$, where we define

$$\begin{aligned}\rho_s(\vartheta; D, r) := r &\left\{ \int_0^1 d\varphi \ \exp\left[-\frac{1}{D}\left[\omega\varphi + \Psi(0,\varphi)r\right]\right] \right\}^{-1} \\ &\times \int_0^1 d\varphi \ \exp\left[-\frac{1}{D}\left[\omega\varphi + \Psi(\vartheta,\vartheta+\varphi)r\right]\right].\end{aligned}$$

By Proposition 2.3, $A_D(r_0) \to A_0(r_0)$ as $D \to 0^+$, with $r_0 \in J_2$ being the fixed point of A_0. Together with the estimate

$$|r_D - r_0| = |A_D(r_D) - A_0(r_0)| \leq L_A\,|r_D - r_0| + |A_D(r_0) - A_0(r_0)| \tag{2.15}$$

this implies that $r_D \to r_0$ as $D \to 0^+$. Furthermore, in a way similar to the proof of Proposition 2.2, one finds that $\rho_s(\vartheta; D, r)$ is Lipschitz continuous in $r \in J_\beta$, with a Lipschitz constant L_r uniform in $D > 0$ and $\vartheta \in S^1$. Denote

$$\rho_s(\vartheta; 0, r) := \frac{r\omega}{\omega + \psi(\vartheta) r}$$

for $\vartheta \in S^1$ and $r \in J_\beta$. Then by (2.2), $\rho_s(\cdot\,; 0, r_0)$ is the stationary state for noise-free networks. Similarly to Proposition 2.3 one finds that $\rho_s(\vartheta; D, r) \to \rho_s(\vartheta; 0, r)$ as $D \to 0^+$ for every $r \in J_\beta$ and $\vartheta \in S^1$. Using the estimate

$$|\rho_s(\vartheta; D, r_D) - \rho_s(\vartheta; 0, r_0)| \leq \; L_r\, |r_D - r_0| + |\rho_s(\vartheta; D, r_0) - \rho_s(\vartheta; 0, r_0)|\,,$$

we conclude that $\rho_s(\vartheta; D, r_D) \to \rho_s(\vartheta; 0, r_0)$ as $D \to 0^+$ for every $\vartheta \in S^1$. It remains to show the continuous dependence of ρ_s on $D > 0$. For $D, D' > 0$ and the corresponding stationary stimuli r_D, $r_{D'}$, one can estimate

$$(1 - L_A)\, |r_D - r_{D'}| \leq |A_D(r_D) - A_{D'}(r_D)| \tag{2.16}$$

in a fashion similar to (2.15). From (2.9) it is clear that the right-hand side of (2.16) vanishes as $D' \to D$. Since $L_A < 1$, this implies that $r_D \to r_{D'}$ as $D' \to D$. Consequently, $\rho_s(\vartheta; D, r_D) \to \rho_s(\vartheta; D', r_{D'})$ as $D' \to D$, uniformly in $\vartheta \in S^1$. ∎

Lemma 2.5. *For any $\mathcal{E}_m > 0$ and $r_m > 1$ there exists a constant $C > 0$ such that whenever $\mathcal{E} := \|\psi\|_\infty / \omega \leq \mathcal{E}_m$ and $D/\omega \geq C$, there exists exactly one stationary state $\rho_s \in \mathcal{C}^2(S^1, \mathbb{R})$ with $\rho_s(0) \in [0, r_m]$. Furthermore, $\rho_s(\vartheta) \to 1$ as $D/\omega \to \infty$ uniformly in $\vartheta \in S^1$ and $\mathcal{E} \leq \mathcal{E}_m$.*

Proof. From (2.9) it is straightforward to show that the derivative $A_D'(r)$ of the functional A_D tends to 0 as $D/\omega \to \infty$, uniformly in $\mathcal{E} \leq \mathcal{E}_m$ and $r \in [0, r_m]$. Now choose $C > 0$ so large that $A_D'|_{[0,r_m]} < \min\{1, (r_m - 1)/r_m\}$ whenever $D/\omega \geq C$ and $\mathcal{E} \leq \mathcal{E}_m$. Since $A_D(0) = 1$, we find that A_D has a unique fixed point in $[0, r_m]$ whenever $D/\omega \geq C$ and $\mathcal{E} \leq \mathcal{E}_m$, corresponding to the stimulus $\rho_s(0)$ of a stationary state $\rho_s \in \mathcal{C}^2(S^1)$. Furthermore, $\rho_s(0) \to 1$ as $D/\omega \to \infty$ uniformly in $\mathcal{E} \leq \mathcal{E}_m$. Recall that by (2.8) we have the representation

$$\rho_s(\vartheta) = \frac{\rho_s(0)}{M(\rho_s(0))} \int_0^1 d\varphi\; e^{-\frac{\omega}{D} V(\vartheta, \varphi, \rho_s(0))}.$$

We conclude that $\rho_s(\vartheta) \to 1$ as $D/\omega \to \infty$, uniformly in $\vartheta \in S^1$ and $\mathcal{E} \leq \mathcal{E}_m$. ∎

The last two lemmas describe the local qualitative change of stationary states in noisy networks as noise tends to zero or to infinity. They show that, for weak coupling, the stationary state is preserved in a modified form as noise is increased from zero, and tends to the uniform distribution as noise tends to infinity. Contrary to the noise-free case (Lemma 2.1), this preserved stationary state is only locally unique, and in fact little information is provided on the possible appearance of other stationary states. Nonetheless, the radius of uniqueness (in the supremum norm) can be chosen large enough, provided that coupling is sufficiently weak or noise sufficiently strong.

3. Stability of stationary states.

In this section we perform a linear stability analysis of stationary states ρ_s against small perturbations $h(t) \in \mathcal{C}^1(S^1)$.

3.1. Stability analysis in noise-free networks. We start with the case $D = 0$. Suppose $\rho_s + h$ satisfies the Fokker–Planck equation (1.1). It is then easy to see that h satisfies the evolution equation

$$\partial_t h(t,\vartheta) = (\mathcal{Q}h(t,\cdot))(\vartheta) - h(t,0)\cdot(h(t,\vartheta)\psi(\vartheta))', \tag{3.1}$$

where the linear operator $\mathcal{Q}$ is given by

$$\mathcal{Q}f = -\left[(\omega + \psi\rho_s(0))\cdot f\right]' - (\psi\rho_s)' f(0), \qquad f \in \mathcal{C}^1(S^1),$$

with the prime symbol denoting the partial derivative with respect to $\vartheta \in S^1$. Note that $\mathcal{Q}$ maps $\mathcal{C}^1(S^1)$ into the space $\mathcal{C}_{\mathrm{zm}}(S^1)$ of continuous functions with zero mean. In fact, in view of the normalization condition $\int_{S^1}(\rho_s + h) = 1$ imposed on all network states, we will consider only the restriction of $\mathcal{Q}$ to the domain $\mathcal{C}^1_{\mathrm{zm}}(S^1)$, the latter seen as a subspace of $\mathcal{C}_{\mathrm{zm}}(S^1)$. Determining eigenperturbations h that evolve as $h(t) \approx e^{\lambda t}h(0)$ in the linear approximation corresponds to a point-spectral analysis of $\mathcal{Q}$ and gives insight into the local stability of ρ_s.

Lemma 3.1. *The linear operator $\mathcal{Q}$ has the following properties:*

1. *The point spectrum $\sigma_p(\mathcal{Q})$ is given by the solutions $\lambda \in \mathbb{C}$ of the eigenvalue equation*

$$\int_0^1 d\vartheta\ \frac{e^{\lambda T_s(\vartheta)}}{\mathrm{v}_s^2(\vartheta)} = 0, \tag{3.2}$$

with the so-called stationary velocity $\mathrm{v}_s(\vartheta) := \omega + \psi(\vartheta)\cdot\rho_s(0)$ *and* stationary travel time $T_s(\vartheta) := \int_0^\vartheta d\varphi\ 1/\mathrm{v}_s(\varphi)$. *All eigenvalues are of geometric multiplicity one.*

2. *The eigenvalue equation (3.2) has a countably infinite number of solutions $\{\lambda_n\}_{n\in\mathbb{Z}}$, which can be numbered so that $\lambda_n \sim i2\pi n/T_s(1)$ as $|n| \to \infty$. Furthermore, all eigenvalues satisfy $|\Re(\lambda_n)| \le \rho_s(0)\cdot\|\psi'\|_\infty$.*

Proof. 1. The eigenvalue equation in the eigenperturbation $h \in \mathcal{C}^1_{\mathrm{zm}}(S^1)$ with eigenvalue λ reads

$$(\omega + \psi\rho_s(0))h' + \big(\lambda + \psi'\rho_s(0)\big)\,h + (\psi\rho_s)'h(0) = 0. \tag{3.3}$$

If the perturbation stimulus $h(0)$ is regarded as a fixed parameter, (3.3) is an inhomogeneous linear ODE in h, whose solution is

$$h(\vartheta) = h(0)e^{A_\lambda(\vartheta)}\left[1 + \int_0^\vartheta d\varphi\ B(\varphi)e^{-A_\lambda(\varphi)}\right], \tag{3.4}$$

where

$$A_\lambda(\vartheta) := -\int_0^\vartheta \frac{d\varphi}{\mathrm{v}_s(\varphi)}\left[\psi'(\varphi)\rho_s(0) + \lambda\right],$$
$$B(\vartheta) := -\frac{(\psi\rho_s)'(\vartheta)}{\mathrm{v}_s(\vartheta)} = \frac{\omega\rho_s'(\vartheta)}{\mathrm{v}_s(\vartheta)\rho_s(0)}.$$

The periodicity condition $h(0) = h(1) \neq 0$ is equivalent to

$$\chi(\lambda) := 1 - e^{A_\lambda(1)}\left[1 + \int_0^1 d\varphi\ B(\varphi)e^{-A_\lambda(\varphi)}\right] = 0. \tag{3.5}$$

Note that by the stationary state equation (2.3) we have $T_\mathrm{s}(1) = 1/(\mathrm{v_s}(0)\rho_\mathrm{s}(0))$ and

$$A_\lambda(\vartheta) = \ln \frac{\mathrm{v_s}(0)}{\mathrm{v_s}(\vartheta)} - \lambda T_\mathrm{s}(\vartheta) \tag{3.6}$$

for $\vartheta \in [0,1]$. Every nontrivial solution λ of (3.5) corresponds through (3.4) to a function $h_\lambda \in \mathcal{C}^1(S^1)$ solving (3.3). Since $\lambda h_\lambda = \mathcal{Q}h_\lambda$ is in $\mathcal{C}_\mathrm{zm}(S^1)$ and $\lambda \neq 0$, we have that $h_\lambda \in \mathcal{C}^1_\mathrm{zm}(S^1)$, so that h_λ is an eigenperturbation with eigenvalue λ. The value $\lambda = 0$ always solves (3.5); however, it can be shown to correspond to a perturbation with nonzero mean, given $h_0(0) \neq 0$. It follows that the eigenvalues of $\mathcal{Q}$ are exactly the nontrivial solutions λ of (3.5). Using (3.6) and (2.2), we find that

$$\chi(\lambda) = e^{-\lambda T_\mathrm{s}(1)} \lambda\omega \int_0^1 d\varphi \, \frac{e^{\lambda T_\mathrm{s}(\varphi)}}{\mathrm{v_s}^2(\varphi)}.$$

Thus the nontrivial roots of χ are exactly the solutions of (3.2). The single multiplicity of eigenvalues is evident from (3.4).

2. The eigenvalue equation (3.2) can be brought into the form of a standard exponential integral

$$\int_0^{T_\mathrm{s}(1)} dt \, f(t) e^{\lambda t} = 0, \tag{3.7}$$

with $f(t) := 1/\mathrm{v_s}(\Theta(t))$ and $\Theta : \mathbb{R} \to S^1$ being the solution of the initial value problem

$$\dot{\Theta}(t) = \mathrm{v_s}(\Theta(t)), \quad \Theta(0) = 0.$$

Note that $\Theta(T_\mathrm{s}(1)) = \Theta(0)$. One has $-f'(t)/f(t) = \rho_\mathrm{s}(0)\psi'(\Theta(t))$. By [38, sect. 4] we know that any solution to (3.7) must therefore satisfy $|\Re(\lambda)| \leq \rho_\mathrm{s}(0) \left\|\psi'\right\|_\infty$. Furthermore, defining $\nu(\varphi) := f\left[T_\mathrm{s}(1)(\varphi+1)/2\right]/f(0)$ allows us to write (3.7) in the equivalent form

$$\int_{-1}^1 d\varphi \, \nu(\varphi) e^{\frac{\lambda}{2} T_\mathrm{s}(1)\varphi} = 0, \tag{3.8}$$

with $\nu(-1) = \nu(1) = 1$. It is a known fact [28, Theorem 13] that the zeros $(\lambda_n)_{n\in\mathbb{Z}}$ of (3.8) can be numbered in such a way that $\lambda_n T_\mathrm{s}(1)/2 \sim n\pi i$ as $|n| \to \infty$. ■

Note that $T_\mathrm{s}(\vartheta)$ is the time it takes for an oscillator to advance from phase 0 to ϑ when the network is in stationarity. Assertion 2 of Lemma 3.1 can be interpreted in the following way: Eigenperturbations of high orders (high frequencies) oscillate at frequencies which are approximately integer multiples of the *stationary oscillator frequency* $1/T_\mathrm{s}(1)$. Furthermore, they tend to have slow dynamics, decaying or growing at a rate approaching zero as their order tends to infinity. Lemma 3.2 below takes this finding to an extreme for response functions having a symmetry property. We note that spectra approximating the grid $i2\pi/T_\mathrm{s}(1)\cdot\mathbb{Z}$ have also been found in the stability analysis of stationary states for similar networks with smooth (as opposed to Dirac-like) pulses in the limit of weak coupling [1].

Lemma 3.2. *Suppose the response ψ satisfies $\psi(\vartheta) = \psi(-\vartheta)$ for all $\vartheta \in S^1$. Then either all eigenvalues of $\mathcal{Q}$ are purely imaginary, or all but a finite number of eigenvalues are purely*

imaginary and some eigenvalues have strictly positive real part. In particular, the stationary state is either (linearly) neutrally stable or unstable.

Proof. We begin with a claim: If $\lambda = x + iy$ (with $x, y \in \mathbb{R}$) solves the eigenvalue equation (3.2), then so does its reflection $\tilde{\lambda} := -x + iy$. To prove the claim, note that $\mathrm{v_s}(\vartheta) = \mathrm{v_s}(1-\vartheta)$ and thus $T_\mathrm{s}(\vartheta) = T_\mathrm{s}(1) - T_\mathrm{s}(1-\vartheta)$ for $\vartheta \in [0,1]$. Therefore,

$$\begin{aligned}\int_0^1 d\vartheta\ \frac{e^{\tilde{\lambda}T_\mathrm{s}(\vartheta)}}{\mathrm{v_s^2}(\vartheta)} &= e^{\tilde{\lambda}T_\mathrm{s}(1)} \int_0^1 d\vartheta\ \frac{e^{\lambda^* T_\mathrm{s}(1-\vartheta)}}{\mathrm{v_s^2}(\vartheta)} = e^{\tilde{\lambda}T_\mathrm{s}(1)} \int_0^1 d\vartheta\ \frac{e^{\lambda^* T_\mathrm{s}(\vartheta)}}{\mathrm{v_s^2}(1-\vartheta)} \\ &= e^{\tilde{\lambda}T_\mathrm{s}(1)} \left[\int_0^1 d\vartheta\ \frac{e^{\lambda T_\mathrm{s}(\vartheta)}}{\mathrm{v_s^2}(\vartheta)}\right]^* = 0.\end{aligned}$$

Now suppose $\sigma_\mathrm{p}(\mathcal{Q})$ is not purely imaginary. Then by the above claim, at least one eigenvalue has strictly positive real part. Furthermore, due to the asymptotic distribution of eigenvalues for large orders predicted by Lemma 3.1(2), only a finite number of eigenvalues λ_n admits a reflection $\tilde{\lambda}_n \neq \lambda_n$. ∎

3.2. Stability analysis in networks with noise. In analogy to noise-free networks, a good starting point for a local stability analysis of stationarity in noisy networks would be the linearized dynamics of small perturbations $h(t) \in \mathcal{C}^2_\mathrm{zm}(S^1)$. Similarly to (3.1) one finds the dynamics

$$\partial_t h = \mathcal{Q}_D h - h(0)(h\psi)'$$

with the linear part

$$\mathcal{Q}_D h := -(\mathrm{v_s} h)' - (\psi\rho_\mathrm{s})' h(0) + Dh''$$

provided that $\rho_\mathrm{s} + h$ satisfies the Fokker–Planck equation (1.1). Note that $\mathcal{Q}_D$ maps $\mathcal{C}^2(S^1)$ into $\mathcal{C}_\mathrm{zm}(S^1)$. Unlike in the noise-free case, the eigenvalue equation $\mathcal{Q}_D h = \lambda h$ is not easily reducible to a lower dimensional form.

One may attempt to deal with the eigenvalue equation through a trigonometric approximation of eigenperturbations. The condition $Dh'' = \lambda h + (\mathrm{v_s} h)' + (\psi\rho_\mathrm{s})' \cdot h(0)$ implies that any eigenperturbation $h \in \mathcal{C}^2_\mathrm{zm}(S^1)$ is in fact in $\mathcal{C}^3_\mathrm{zm}(S^1)$ (recall that by section 2.2 one has $\rho_\mathrm{s} \in \mathcal{C}^2(S^1)$). Thus the Fourier series of h, h', and h'' converge uniformly. It is straightforward to see that the eigenvalue equation $\mathcal{Q}_D h = \lambda h$ is equivalent to the algebraic system

$$\begin{aligned}\lambda \mathcal{F}_n(h) = &-(2\pi n)^2 D \mathcal{F}_n(h) \\ &- i2\pi n \sum_{k=-\infty}^{\infty} \mathcal{F}_k(h)\mathcal{F}_{n-k}(\mathrm{v_s}) \\ &- i2\pi n \mathcal{F}_n(\psi\rho_\mathrm{s}) \sum_{k=-\infty}^{\infty} \mathcal{F}_k(h)\end{aligned} \tag{3.9}$$

for $n \in \mathbb{Z} \setminus \{0\}$, with $\mathcal{F}_0(h) = 0$. The above system is the starting point for the approximative method used in the numerical spectral stability analysis presented in section 4.2 below.

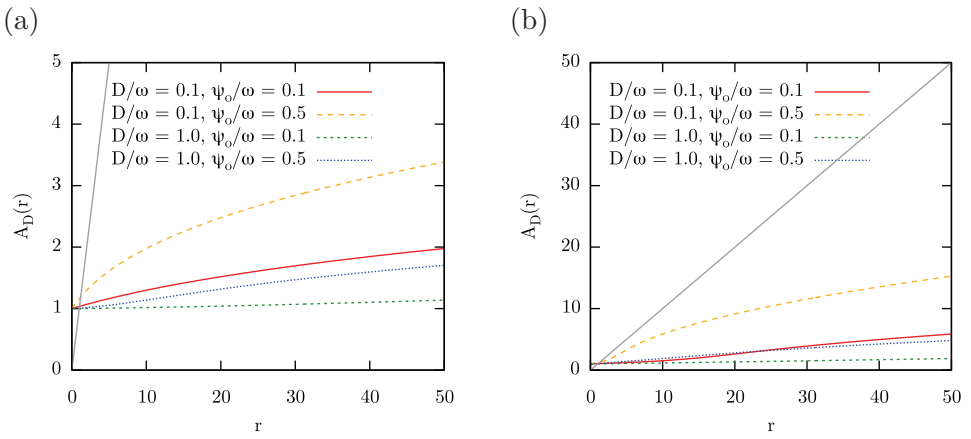

Figure 2. *Graph of the function A_D introduced in Proposition 2.2 for* (a) *symmetric accelerating type* I *and* (b) *symmetric attracting type* II *responses. The solid line is the diagonal in $\mathbb{R}^2_+$. Fixed points of A_D correspond to stationary stimuli. Note that all graphs intersect the diagonal exactly once and within the interval $[0, 2]$. This property is shared by all symmetric and nonsymmetric type* I *and type* II *responses that we tested.*

4. Numerical methods. In this section we outline the numerical methods we used to further investigate the model (1.1). These methods involve the solution of the stationary state equations, the calculation of the point spectrum of the linearized dynamics at stationary states, and the integration of the Fokker–Planck equation. Technical details are given in Appendix B. The numerical analysis was applied exclusively to type I and type II responses (1.4)–(1.5). We restricted our attention to the parameter values $\vartheta_o \in [0.3, 0.7]$, $|\psi_o|/\omega \in [0, 0.5]$, and $D/\omega \in [0, 1]$. In our calculations we normalized $\omega = 1$, though we use the dimensionless parameters ψ_o/ω and D/ω for the presentation of the results.

4.1. Evaluating the stationary state equations. Both stationary state equations (2.3) and (2.9) are generally difficult to solve analytically. In order to get a better feeling for the shapes of stationary states and their dependence on the response function and noise strength, we implemented numerical quadratures of the integral expressions involved. Using them, we constructed routines for the evaluation of the operator A_D introduced in Lemma 2.1 ($D = 0$) and Proposition 2.2 ($D > 0$). We were thus able to search for stationary states (or rather their corresponding stimuli) using a fixed-point iteration of A_D, as suggested by Proposition 2.2 for both type I and type II responses. We refer the reader to Appendix B.1 for technical details. Figure 2 shows a numerical evaluation of the functional A_D for symmetric type I and type II responses and typical combinations of D/ω and ψ_o/ω. As can be seen, the graph of the functional $A_D : \mathbb{R}_+ \to \mathbb{R}_+$ intersects, at least within the illustrated domain, the diagonal exactly once. This suggests the uniqueness of the calculated stationary states.

4.2. Evaluating the eigenvalue equations. For the linear stability analysis of stationarity in noise-free networks, the eigenvalue equation (3.2) for the operator $\mathcal{Q}$ (see section 3.1) was solved numerically as described in Appendix B.2. For the spectral stability analysis of stationarity in noisy networks, our starting point was the infinite system of equations (3.9) in the Fourier spectrum of eigenperturbations, introduced in section 3.2. For its numerical

evaluation we considered only a finite subset of it by implicitly assuming $\mathcal{F}_n(h) = 0$ for $|n| > N$ (for some sufficiently large N) for the sought eigenperturbations $h \in \mathcal{C}^2_{\mathrm{zm}}(S^1)$. See Appendix B.3 for more technical details. The results of this approach agree very well with those of the exact spectral analysis for the special case $D = 0$.

4.3. Integrating the Fokker–Planck equation. In order to better understand the behavior of the network near stationary states and also determine other possible attractors, we numerically integrated the Fokker–Planck equation (1.1). For that we used a so-called *spectral method* (see [2, sect. 3.C] for a review of this approach to the Kuramoto model). The idea is to approximate the density $\rho(t, \vartheta)$ by a finite trigonometric sum in ϑ of sufficiently high order. The time-dependent Fourier coefficients then satisfy a finite system of ODEs, which can be solved using standard tools. We refer the reader to Appendix B.4 for technical details.

5. Behavior for type I responses. We now focus on the structure and stability of stationary states as well as the long term behavior of the model for type I responses defined by (1.4), using the numerical methods outlined in section 4. Our stability analysis shows that a sufficiently strong noise locally stabilizes stationarity. Numerical simulations in fact suggest this stability to be global. As noise is reduced, stationarity undergoes a supercritical Hopf bifurcation, and a stable limit cycle appears, the so-called *main attractor*, on which the network splits up into several approximately synchronized oscillator groups. The system's long term behavior seems to be dominated by the attractor consisting of the stationary state, the main attractor, and the orbits connecting the two.

5.1. Stationary states and stationary stimuli. For noise-free networks with symmetric type I responses $\psi(\vartheta) = \frac{\psi_o}{2}\,[1 - \cos(2\pi\vartheta)]$, the stationary state equation (2.3) admits as solution the unique stationary stimulus

$$\rho_{\mathrm{s}}(0) = \frac{\psi_o}{2\omega} + \sqrt{\left(\frac{\psi_o}{2\omega}\right)^2 + 1}. \tag{5.1}$$

Solving the stationary state equation for networks with noise or nonsymmetric responses turns out to be more difficult; hence we resort to numerical methods as described in section 4.1. Figure 3(a) shows typical stationary states in networks with symmetric accelerating type I responses and various noise strengths. For delaying symmetric responses, stationary states qualitatively follow a similar pattern, though with swapped minima and maxima. For nonsymmetric responses, stationary states change accordingly. We note that, contrary to the Kuramoto model [25, 26], the stationary phase distribution here is far from being uniform.

In view of the interpretation of the stimulus $\rho(t, 0)$ as current *network activity*, the dependence of the stationary stimulus $\rho_{\mathrm{s}}(0)$ on parameters like the coupling strength $|\psi_o|/\omega$ and noise strength D/ω are of special interest. Figures 3(b) and 3(c) illustrate how $\rho_{\mathrm{s}}(0)$ varies with these parameters for symmetric type I responses. Figure 3(b) shows that for accelerating responses, increased coupling and weaker noise lead to a higher stationary network activity. For delaying responses, on the other hand, increased coupling and weaker noise lead to a lower stationary network activity, as shown in Figure 3(c). Similar relations were found to hold for nonsymmetric type I responses as well.

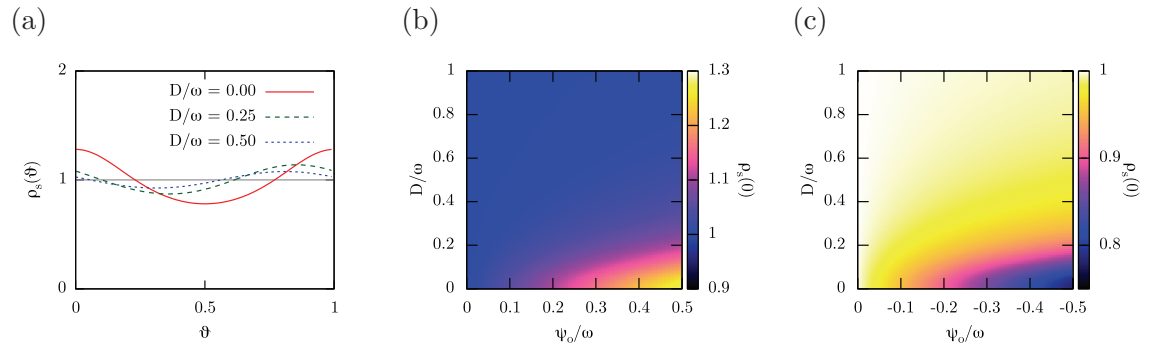

Figure 3. (a) *Stationary states in networks with symmetric accelerating type* I *responses and coupling strength* $|\psi_o|/\omega = 0.5$. *The horizontal line represents the uniform distribution approached in the limit* $D/\omega \to \infty$. (b) *and* (c) *Stationary stimuli* $\rho_s(0)$ *for various coupling and noise strengths for accelerating* (b) *and delaying* (c) *symmetric type* I *responses. Note the different value ranges.*

5.2. Linear stability of stationarity. For noise-free networks with symmetric type I responses, the eigenvalue equation (3.2) for the linearized dynamics at ρ_s can be treated analytically (see Appendix C). As it turns out, the point spectrum is purely imaginary and given by

$$\sigma_p(\mathcal{Q}) = \left\{ \lambda_n := \frac{i2\pi n}{T_s(1)} : n \in \mathbb{Z} \setminus \{0, \pm 1\} \right\} \cup \left\{ \lambda_{\pm 1} := \pm i\omega 2\pi \sqrt{1 + \frac{\psi_o}{2\omega}\rho_s(0)} \right\}. \tag{5.2}$$

Compare this to the predictions of Lemmas 3.1(2) and 3.2. Eigenperturbations h_n of *order* n corresponding to eigenvalues λ_n are characterized by $|n|$ local maxima and $|n|$ local minima in their real as well as imaginary parts. Each one can be interpreted as tending to split oscillators into $|n|$ synchronized groups. As eigenvalues appear in complex-conjugate pairs, only those with nonnegative imaginary parts will be considered in the following.

Since all eigenvalues have zero real part, stationary states in noise-free networks with symmetric type I responses are only (linearly) neutrally stable. It turns out, though, that the symmetric case ($\vartheta_o = 0$) is a special one, since for both $\vartheta_o < 0.5$ and $\vartheta_o > 0.5$ at least two eigenvalues are found on the right half plane, leading to the instability of stationarity. Figures 4(a) and (b) show the computed spectra for $|\psi_o|/\omega = 0.5$ and different turning points ϑ_o. Figures 5(a) and (b) further illustrate the dependency of the real part of eigenvalues on ϑ_o. Figure 4(c) shows typical leading eigenperturbations in networks with accelerating type I responses. It is apparent that these differ qualitatively for the cases $\vartheta_o < 0.5$ and $\vartheta_o > 0.5$, corresponding to different orders. A similarly abrupt change of leading eigenvalue order also appears for delaying type I responses. Integrating the Fokker–Planck equation (1.1) reveals that this difference is related to a bifurcation in the long term behavior of the network as ϑ_o passes through 0.5 (see section 5.3 below).

As noise is increased, all eigenvalues move toward the left half plane at a speed increasing with their order. For sufficiently strong noise, all eigenvalues are eventually located on the open left half plane, suggesting a local stabilization of stationarity. This is illustrated in Figures 5(c)–(d), which show the stability spectra of stationary states over varying ϑ_o and

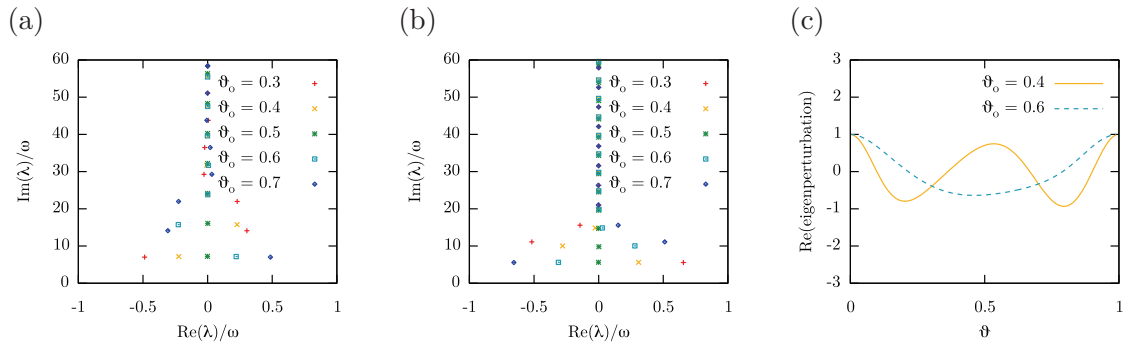

Figure 4. *Stability spectra of stationary states in noise-free networks with* (a) *accelerating and* (b) *delaying type* I *responses for various turning points* ϑ_o. (c) *Leading eigenperturbations (real part) of stationary states in noise-free networks with accelerating type* I *responses. Leading eigenvalues are* $\lambda \approx (0.23 + i \cdot 15.75)\omega$ *(order* 2*) for* $\vartheta_o = 0.4$ *and* $\lambda \approx (0.22 + i \cdot 7.18)\omega$ *(order* 1*) for* $\vartheta_o = 0.6$. *Eigenperturbations are scaled to have value* 1 *at the origin. Their imaginary part is of shape similar to that of their real part. Coupling strength is* $|\psi_o|/\omega = 0.5$ *in all cases.*

nonzero noise. While a noise-induced stabilization takes place regardless of ϑ_o and the coupling strength, the exact noise threshold depends nontrivially on both, as is illustrated in Figures 6(a)–(b). They show the real part of leading eigenvalues over varying coupling and noise strengths for fixed $\vartheta_o = 0.4$. As can be seen, stationarity becomes stable when noise exceeds a certain threshold, which itself increases (weakly nonlinearly) with the coupling strength.

5.3. Numerical simulations. The stability of stationarity as well as the long term behavior of networks have been tested by integrating the Fokker–Planck equation (1.1) as described in section 4.3. Parameter values considered were $\vartheta_o \in \{0.3, 0.4, 0.6, 0.7\}$, $|\psi_o|/\omega \in \{0.1, 0.5\}$, and $D/\omega \in [0, 1]$. The local stability of stationarity has been tested against eigenperturbations h (real part) of order up to 10, with $\|h\|_\infty \approx 0.01$. Other applied perturbations included random harmonic ones of order up to 10 with similar amplitudes.

Our simulations reproduce the predictions of the linear stability analysis. More precisely, in the unstable realm, all applied perturbations result in the network splitting up into n oscillator groups, with n being the order of the leading eigenvalue λ_n (e.g., two for $\vartheta_o = 0.4$, $\psi_o/\omega = 0.5$, $D = 0$). Eventually, the network settles on a limit cycle, on which all oscillators in each of these n (approximately equally sized) groups are in partial synchrony. The degree of synchrony within each group increases with decreasing noise, and for zero noise each group is perfectly synchronized. This splitting of the network into successively firing oscillator groups results in an oscillation of the network stimulus at a frequency near $\Im(\lambda_n)/(2\pi)$. We mention that initial distributions near a uniform or Gaussian distribution also eventually converge to this limit cycle, though in some cases after a transition close to stationarity, indicating a large basin of attraction. We shall therefore refer to this limit cycle as the *main attractor*. In fact, our simulations suggest that the main attractor, the stationary state, and the orbits connecting the two constitute a global attractor.

Figure 7(a) shows the results of such a simulation for $\vartheta_o = 0.4$, $\psi_o/\omega = 0.5$, and zero noise. It demonstrates the splitting of the network into two groups, the oscillators within each group

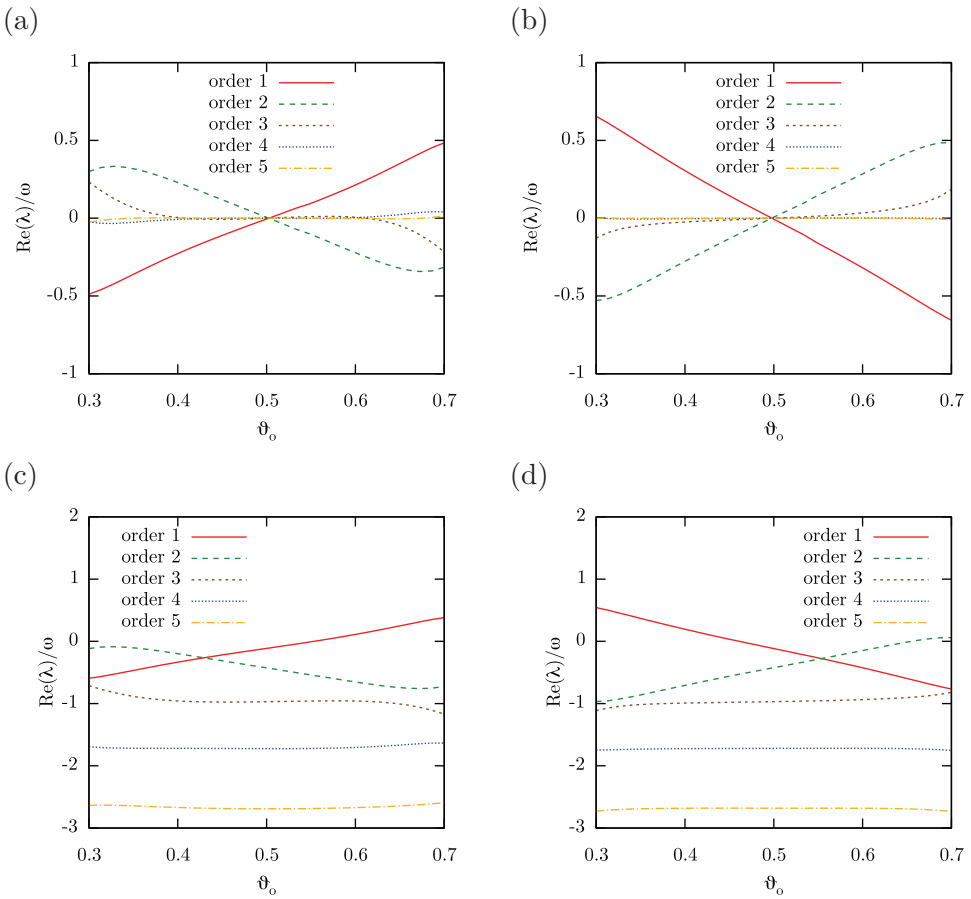

Figure 5. *Real parts of low-order eigenvalues for type* I *responses (accelerating in the left column and delaying in the right column) as a function of the turning point ϑ_o for two different noise levels ($D = 0$ in the top row and $D/\omega = 0.0025$ in the bottom). Only the first five eigenvalue orders (including the leading ones) are displayed. Increasing the noise shifts all eigenvalues to the left half plane (lower real part) at a rate increasing with the eigenvalue order. The coupling strength is $|\psi_o|/\omega = 0.5$, but similar results have also been found for $|\psi_o|/\omega \in \{0.1, 0.2, \ldots, 0.5\}$.*

being in synchrony. Figure 7(b) depicts the evolution of the corresponding network stimulus, oscillating at an ever-increasing amplitude. Figures 8(a)–(c) show typical simulation results for the same response function and nonzero noise, still in the unstable realm and for various initial distributions. The evolution of the corresponding network stimuli is given in Figures 8(d)–(f). In all cases the network is seen to eventually settle on the main attractor.

At a particular threshold noise strength, the main attractor merges with the network's stationary state. This point coincides with the local stabilization of stationarity, as is typical for a supercritical Hopf bifurcation. Figure 9 shows the results of an example integration of the Fokker–Planck equation for networks with accelerating type I responses ($\vartheta_o = 0.4$ and $\psi_o/\omega = 0.5$), with sufficiently strong noise so that stationarity has been stabilized and the main attractor has vanished.

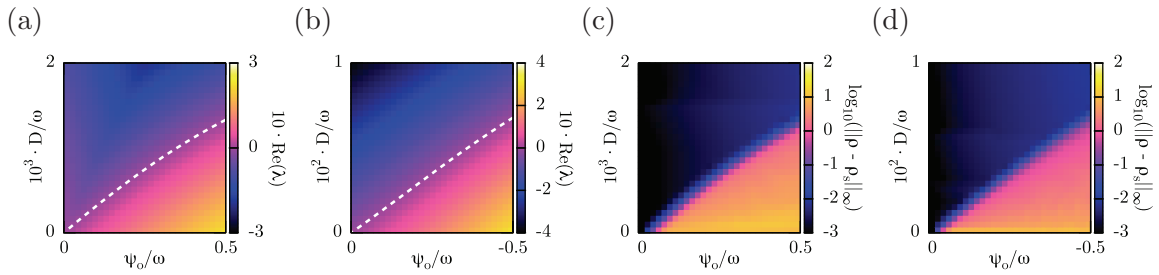

Figure 6. *The similarity between the real part of the leading eigenvalues at stationary states* ((a) *and* (b)), *and the global distance of phase density from stationarity* ((c) *and* (d)), *evaluated over a range of coupling and noise strengths. Responses were* (a)–(c) *accelerating and* (b)–(d) *delaying type* I *responses with* $\vartheta_o = 0.4$. *The white dashed contour is at level zero. Note the different noise scales. The leading eigenvalue is of order* 2 *in* (a), *at least for the unstable parameter range, and of order* 1 *in* (b) *for the whole parameter range. Figures* (c) *and* (d) *show the supremum distance (logarithmic scale) of phase density at time* $t = 200\ \omega^{-1}$ *from stationarity after integration of the Fokker–Planck equation* (1.1) *starting from a uniform distribution. The integration time step was* $2.5 \times 10^{-4}\ \omega^{-1}$, *and the spectral order was* 100. *The supremum distance is evaluated on a uniform grid of size* 100. *Similar spectra and simulation results have also been obtained for* $\vartheta_o = 0.3, 0.4, 0.6,$ *and* 0.7.

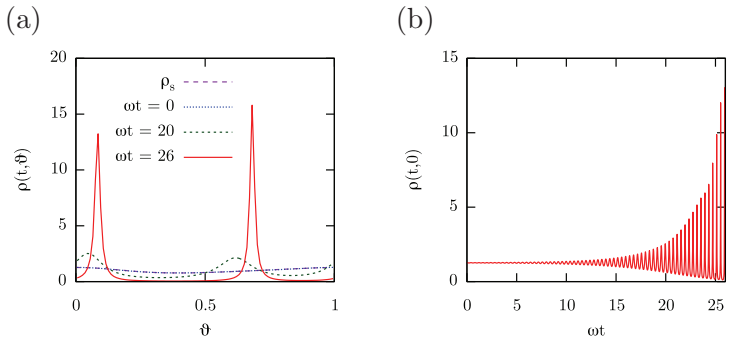

Figure 7. *Integration of the Fokker–Planck equation for networks with accelerating type* I *responses with* $\vartheta_o = 0.4$ *and zero noise.* (a) *Evolution of the phase density after a perturbation of the stationary state. The perturbation was the real part of the leading eigenperturbation* ($\lambda_2 \approx (0.23 + i \cdot 15.75)\omega$, *order* 2) *with perturbation stimulus* 0.01. *Note that the initial and stationary densities seemingly overlap in the graphic.* (b) *Evolution of the corresponding network stimulus. The latter eventually oscillates at a frequency* $(2.52 \pm 0.05)\omega \approx \Im(\lambda_2)/(2\pi)$. *The coupling strength is* $\psi_o/\omega = 0.5$. *The Fokker–Planck equation was integrated as described in section* 4.3 *at spectral order* 300 *and time step* $2 \times 10^{-5}\ \omega^{-1}$.

Our numerical simulations suggest that the local stabilization of stationarity in fact goes along with its global stabilization. We demonstrate this in Figures 6(c) and (d). They show the final distance of the network state to stationarity for accelerating and delaying type I responses, for a range of coupling and noise strengths. The initial distribution in these simulations was the uniform one, but similar results have been obtained for other initial distributions as well (e.g., for wrapped normal distribution with variance $\sigma^2 = 4 \times 10^{-4}$). Notice the narrow transition bands between orders of magnitude in the final distance to stationarity across these maps. These bands closely resemble the transition boundaries in Figures 6(a) and (b) between linear stability and instability. Similar spectra and simulation results have also been obtained

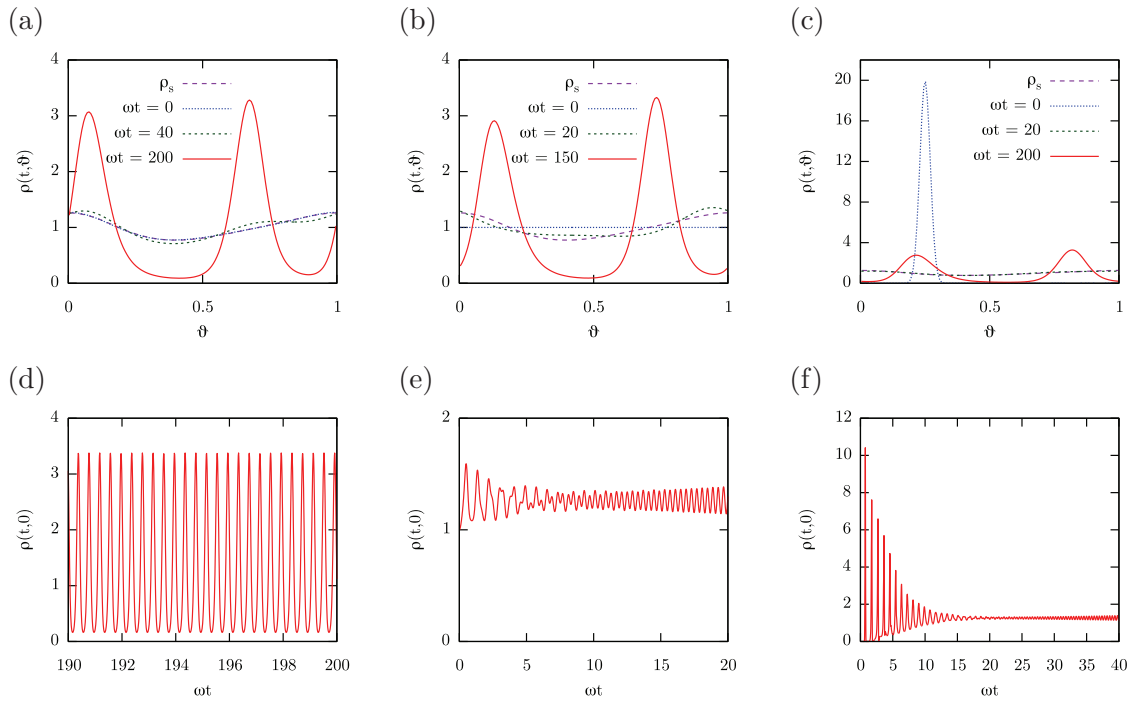

Figure 8. *Example integration of the Fokker–Planck equation for networks with accelerating type* I *responses with turning point* $\vartheta_o = 0.4$ *and weak noise and for various initial distributions. Top row: Evolution of the phase density. Bottom row: Evolution of the stimuli (partially displayed) corresponding to the simulation on top.* (a) *and* (d): *The initial distribution was the stationary state, perturbed by the real part of the leading eigenperturbation (*$\lambda_2 \approx (0.051 + i \cdot 15.75)\omega$*, order* 2*), with a perturbation stimulus* 0.01. (b) *and* (e): *The initial distribution was the uniform one.* (c) *and* (f): *The initial distribution was the wrapped normal distribution* [31, *sect.* 3.5.7] *with variance* $\sigma^2 = 4 \times 10^{-4}$. *In all cases the stimuli eventually approach the form shown in* (d), *oscillating at a frequency* $(2.51 \pm 0.05)\omega \approx \Im(\lambda_2)/(2\pi)$. *These final patterns persist for as long as simulations were run (at least* 10 *times the periods displayed). Note that in* (a) *the initial and stationary densities seemingly overlap. The same is true for the intermediate and stationary densities in* (c). *Also note the different density scales in* (c) *compared to* (a) *and* (b). *Other parameters are* $\psi_o/\omega = 0.5$ *and* $D/\omega = 10^{-3}$. *The Fokker–Planck equation was integrated as described in section* 4.3 *at spectral order* 150 *and time step* $2 \times 10^{-4}\ \omega^{-1}$.

for $\vartheta_o = 0.3$, 0.4, 0.6, and 0.7.

6. Behavior for type II responses. We now consider type II responses defined by (1.5). We study the structure and stability of stationarity and the long term network behavior. To a large extent, type II responses induce behavioral patterns similar to those induced by type I responses. In particular, stationarity is still stabilized by sufficiently strong noise, and the stabilization is accompanied by a supercritical Hopf bifurcation similar to type I responses. The corresponding limit cycle appearing at sufficiently low noise levels, the so-called *main attractor*, is characterized by a splitting of the network into several approximately equally sized and approximately synchronized oscillator groups. The stationary state, the main attractor, and the orbits connecting the two apparently constitute an attractor of the system. In contrast to type I responses, we demonstrate the existence of a second limit cycle for certain type II responses under weak noise.

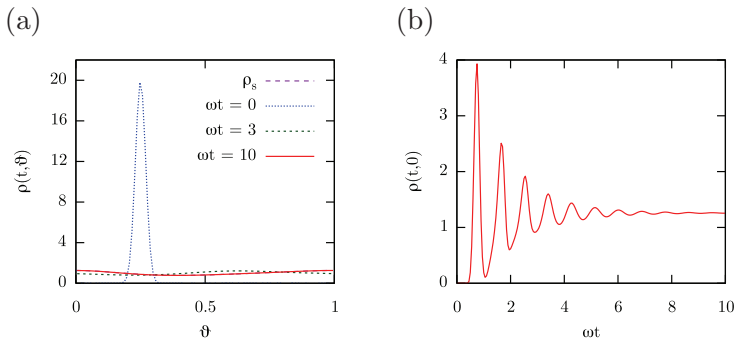

Figure 9. *Integration of the Fokker–Planck equation for accelerating type* I *responses with turning point* $\vartheta_o = 0.4$ *and noise strong enough to stabilize stationarity. The initial distribution was the wrapped normal distribution with variance* $\sigma^2 = 4 \times 10^{-4}$. (a) *Evolution of the phase density.* (b) *Evolution of the network stimulus. Note that in* (a) *the final and stationary densities seemingly overlap. Similar asymptotic behavior was observed for all other tested initial densities (e.g., bimodal and uniform) as well. Coupling and noise strengths are* $\psi_o/\omega = 0.5$ *and* $D/\omega = 10^{-2}$, *respectively. The Fokker–Planck equation was integrated as described in section* 4.3 *at spectral order* 150 *and time step* $2 \times 10^{-4}\ \omega^{-1}$.

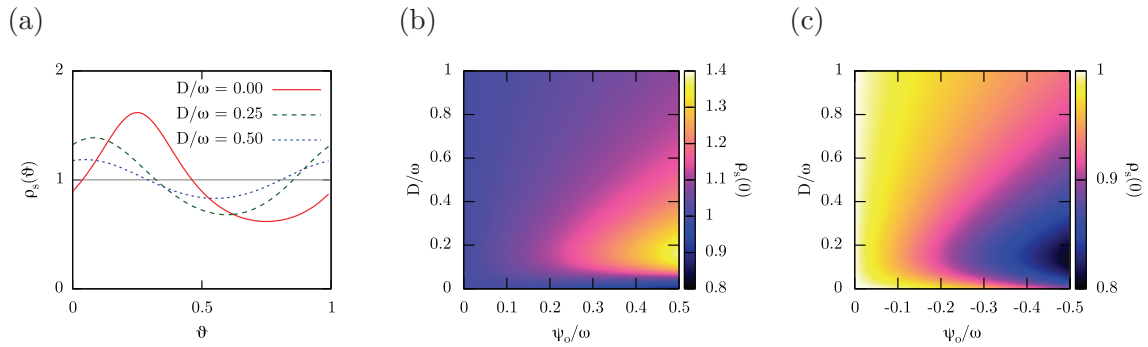

Figure 10. (a): *Stationary states in networks with attracting symmetric type* II *responses with coupling strength* $|\psi_o|/\omega = 0.5$ *and various noise strengths. The horizontal line represents the uniform distribution approached as* $D/\omega \to \infty$. *Stationary stimuli* $\rho_s(0)$ *for various coupling and noise strengths are shown for* (b) *attracting and* (c) *repulsing symmetric type* II *responses. Note the different value ranges.*

6.1. Stationary states and stationary stimuli. For noise-free networks with symmetric type II responses $\psi(\vartheta) = -\psi_o \cdot \sin(2\pi\vartheta)$, the stationary state equation (2.3) has the unique solution

$$\rho_s(0) = \left[1 + (\psi_o/\omega)^2\right]^{-1/2}. \tag{6.1}$$

Stationary states for the case of nonsymmetric responses or nonzero noise had to be calculated numerically as described in section 4.1. Figure 10(a) shows some typical stationary states in networks with attracting, symmetric type II responses for various noise strengths. For repulsing symmetric responses, stationary states qualitatively follow a similar pattern, though with swapped minima and maxima. For nonsymmetric responses, stationary states change accordingly.

Figures 10(b) and (c) illustrate how the stationary stimulus varies with the coupling and noise strengths for symmetric type II responses. For attracting responses, the network's activity depends (for fixed coupling strength) nonmonotonically on the noise strength (Figure 10(b)). In fact, a maximum is attained at a nontrivial noise level—an effect that can be interpreted as a *resonance* between the network's dynamics and noise. For repulsing type II responses, the network's activity depends on the coupling and noise strength in a comparable way (Figure 10(c)), except that here the stationary stimulus is actually minimized at a certain nontrivial noise strength. Similar relations were found to hold for nonsymmetric type II responses as well.

6.2. Linear stability of stationarity. For noise-free networks with symmetric type II responses, the eigenvalue equation (3.2) can be solved analytically (see Appendix D), yielding the point spectrum

$$\sigma_{\mathrm{p}}(\mathcal{Q}) = \left\{ \lambda_n := \frac{i2\pi n}{T_{\mathrm{s}}(1)} : n \in \mathbb{Z} \setminus \{0, \pm 1\} \right\} \cup \left\{ \lambda_{\pm 1} := \pi \left[\psi_o \rho_{\mathrm{s}}(0) \pm \sqrt{\psi_o^2 \rho_{\mathrm{s}}^2(0) - 4\omega^2} \right] \right\}. \tag{6.2}$$

All eigenvalues are purely imaginary except for a pair of complex-conjugate eigenvalues that lie on the open right half plane if $\psi_o > 0$ and on the open left half plane if $\psi_o < 0$. The stationary state ρ_{s} is therefore unstable if $\psi_o > 0$ and (linearly) neutrally stable if $\psi_o < 0$.

Similarly to type I responses, the spectrum always intersects the open right half plane for nonsymmetrical type II responses and sufficiently weak noise. This is illustrated for the case of zero noise in Figures 11(a) and (b). In particular, stationary states are unstable for all attracting responses, unstable for all nonsymmetric repulsing responses, and neutrally stable for symmetric repulsing responses. As with type I responses, eigenperturbations corresponding to eigenvalues of order $n \in \mathbb{N}$ have been found to be characterized by n local maxima and n local minima in their real and imaginary parts. Once again, an increased noise eventually results in the linear stabilization of stationarity, which is illustrated in Figures 11(c) and (d). The eigenvalues move toward the left half plane as noise is increased, with higher order eigenvalues moving faster than lower order ones. The exact noise threshold for stabilization depends nonlinearly on the response parameters, as shown in Figures 12(a) and (b).

6.3. Numerical simulations. The asymptotic behavior of the system has also been studied by integrating the Fokker–Planck equation (1.1) as described in section 4.3. Parameter values considered were $\vartheta_o \in \{0.3, 0.4, 0.6, 0.7\}$ (as well as $\vartheta_o = 0.5$ for attracting responses), $|\psi_o|/\omega \in \{0.1, 0.5\}$, and $D/\omega \in [0, 1]$. Perturbations applied to stationarity were chosen as in section 5.3. The simulations reproduced the predictions of the linear stability analysis.

The observed long term network behavior is similar to that for type I responses. More precisely, we find the existence of a stable limit cycle (henceforth referred to as the *main attractor*), on which the network's state is characterized by a number (henceforth referred to as the *order* of the attractor) of approximately synchronized and approximately equally sized oscillator groups. These groups succeed each other in firing and cause the network's stimulus to oscillate at a constant amplitude and frequency. The level of synchronization within each of these groups increases as noise is reduced. In noise-free networks the main attractor is characterized by a number of perfectly synchronized, equally sized oscillator groups. Simulations indicate that its basin of attraction includes a neighborhood of the stationary state and, in

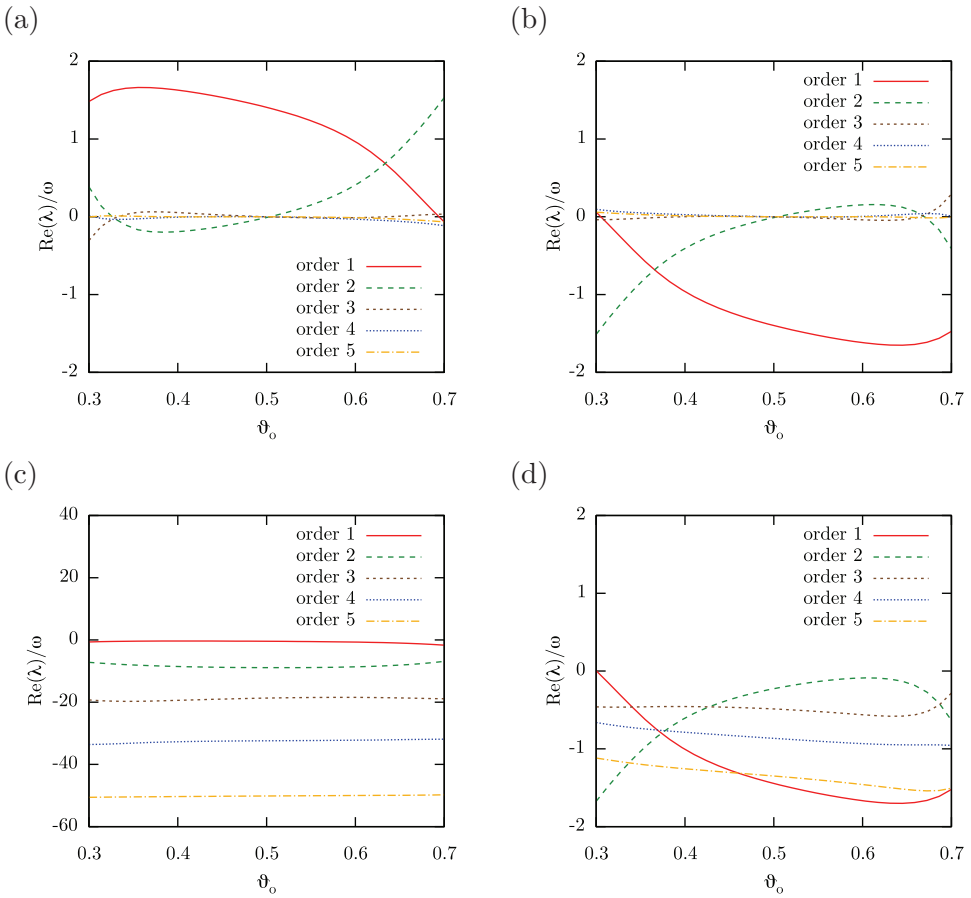

Figure 11. *Real parts of low-order eigenvalues for type* II *responses (attracting in the left column and repulsing in the right column) as a function of the turning point ϑ_o plotted for different noise strengths ($D = 0$ in* (a) *and* (b)*, $D/\omega = 0.05$ in* (c)*, and $D/\omega = 0.001$ in* (d)*). Only the first five eigenvalue orders (including the leading ones) are displayed. Increasing the noise pushes all eigenvalues further to the left half plane (lower real part) at a rate increasing with the eigenvalue order. The coupling strength is $|\psi_o|/\omega = 0.5$, but similar results have been obtained for all coupling strengths $|\psi_o|/\omega \in \{0.1, 0.2, \ldots, 0.5\}$.*

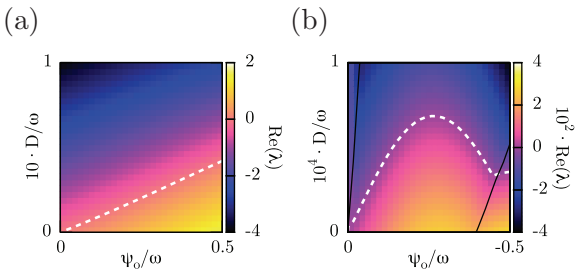

Figure 12. *Real part of the leading eigenvalues of linearized dynamics at stationary states as a function of coupling and noise strength for* (a) *attracting and* (b) *repulsing type* II *responses with turning point $\vartheta_o = 0.4$. The white dashed contour is at level zero. Note the different noise scales. In* (a) *the leading eigenvalue is of order* 1 *in the whole parameter range, whereas in* (b) *the black contours separate the regions where the leading eigenvalue has order* 2 *(leftmost region),* 3 *(center region), and* 4 *(rightmost region).*

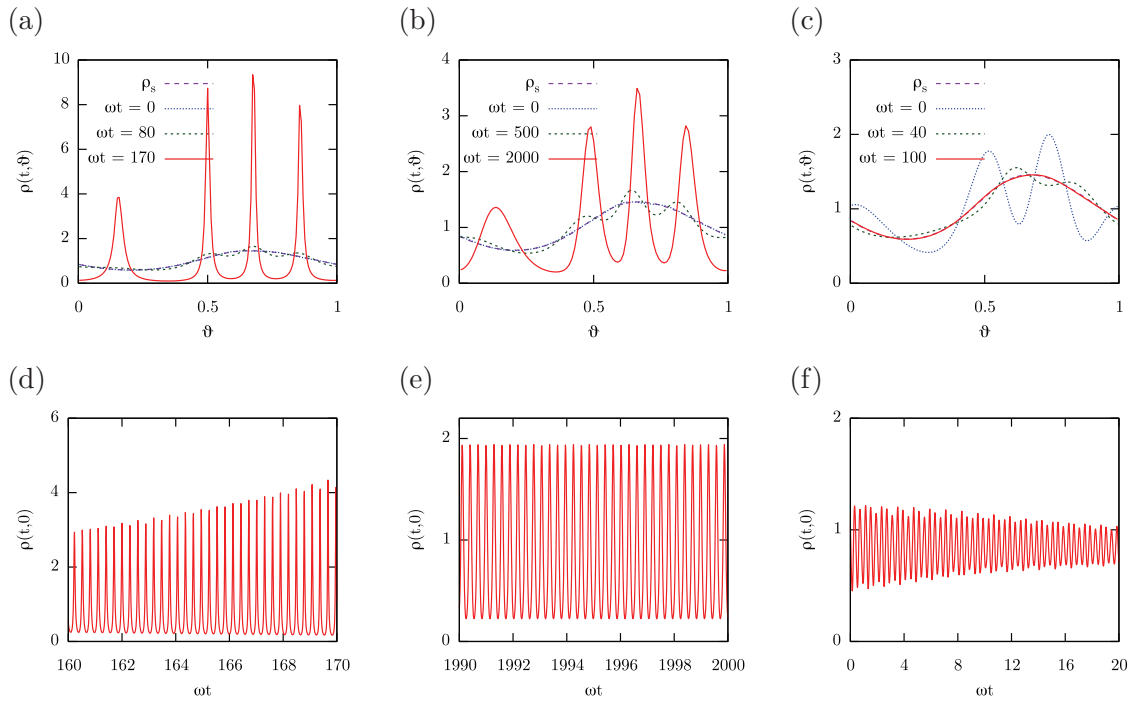

Figure 13. *Integration of the Fokker–Planck equation for repulsing type* II *responses with turning point* $\vartheta_o = 0.4$. *The top row shows the evolution of the phase density after a perturbation of the stationary state for noise level* D/ω *equal to* 0 *in* (a), 3×10^{-5} *in* (b), *and* 10^{-4} *in* (c). *The evolution of the corresponding stimuli is shown in the bottom row below each figure. Perturbations were the real part of the leading eigenperturbations (of order* 4 *in* (a) *and* (b) *and of order* 3 *in* (c)*). Perturbation stimuli were* 0.01 *in* (a)–(b) *and* 0.2 *in* (c). *Note that in* (a) *and* (b) *the initial and stationary densities seemingly overlap. The same is true for the final and stationary densities in* (b). *The coupling strength is* $|\psi_o| / \omega = 0.5$ *in all cases. The Fokker–Planck equation was integrated as described in section* 4.3 *at order* 200 *and time step* $10^{-4}\ \omega^{-1}$.

certain cases, the uniform distribution as well. The order of the main attractor was found to be equal to the order of the leading stationarity eigenperturbation for attracting response functions. For repulsing response functions this was true for most, but not all, cases. When noise strength exceeds a certain threshold, the main attractor merges with the stationary state. This threshold coincides with the point at which stationarity becomes linearly stable, as is characteristic for a supercritical Hopf bifurcation. Our numerical simulations further suggest that at that point stationarity becomes globally stable. This is supported by numerical experiments similar to those for type I responses (section 5.3).

Figure 13 shows typical simulation results for certain nonsymmetric repulsing type II responses starting close to stationarity. In the unstable cases (Figures 13(a)–(b)), the leading eigenvalue is of order four, and oscillators tend to form four clusters that are approximately synchronized. At increasing noise the main attractor vanishes, and stationarity becomes stable (Figure 13(c)).

6.4. Multiplicity of attractors. For certain attracting type II responses and a nontrivial noise range, a second stable limit cycle is found to coexist along with the main attrac-

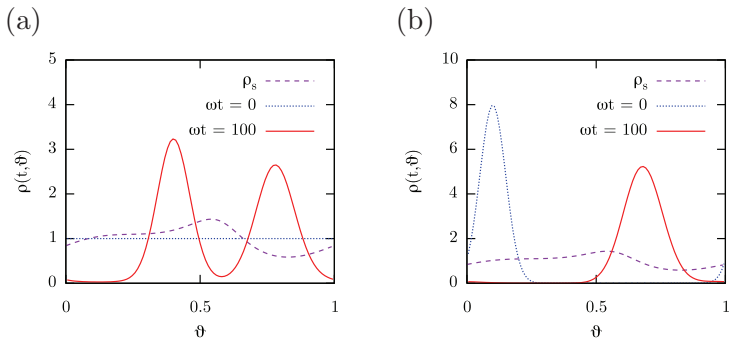

Figure 14. *Coexistence of two stable limit cycles for certain attracting type* II *responses (see section 6.4). The figures show the evolution of the phase density, as predicted by an integration of the Fokker–Planck equation. In* (a) *the network state is initially a uniform distribution, eventually settling on the main attractor, which is characterized by two approximately synchronized oscillator groups. In* (b) *the phase density is initially a wrapped Gaussian with variance* $\sigma^2 = 2 \times 10^{-3}$*, which eventually settles on the secondary attractor, which is characterized by an approximate network synchrony. For comparison, the stationary state is shown with the purple dashed curve. Parameters are* $\vartheta_o = 0.7$*,* $|\psi_o|/\omega = 0.5$*, and* $D/\omega = 0.004$*. The spectral integration order was* 100*, and the time step was* $2 \times 10^{-4}\ \omega^{-1}$*.*

tor described above. This can, for example, be observed for the parameter values $\vartheta_o = 0.7$, $\psi_o/\omega = 0.5$, and $D/\omega \in [0, 0.004]$, for which the leading stationarity eigenperturbation as well as the main attractor are of order 2. Simulations reveal the existence of an additional limit cycle, on which oscillators form a single, more or less synchronized, group. On this *secondary attractor* of *order* 1, the extent of synchrony increases as noise is decreased. In particular, for zero noise, all oscillators are synchronized, and the phase density is formally a time-dependent Dirac distribution. The main attractor's basin of attraction still includes a neighborhood of stationarity as well as the uniform distribution. However, unimodal distributions of an adequately small variance (e.g., wrapped Gaussian with variance $\sigma^2 \lesssim 0.002$) have been found to be included in the basin of attraction of the secondary attractor. The latter vanishes when noise is sufficiently strong but still at a level lower than that needed to destroy the main attractor. See Figure 14 for an illustration of the main and secondary attractors in networks with the above parameter values. These findings suggest that secondary attractors might exist for other response functions as well, at least for weak noise. Under which conditions this is the case, and whether these attractors always disappear before the main attractor as noise is increased, remains to be investigated.

7. Comparing the Fokker–Planck and Langevin equations. As indicated in the introduction, the Fokker–Planck equation (1.1) can be considered a limit of the Winfree model (1.3) extended by additive white noise, as the number of oscillators tends to infinity and the emitted pulses approach a Dirac distribution. To examine the validity of this interpretation, we considered the system of coupled Langevin equations (1.6) in the stochastic processes $\hat{\theta}_1, \ldots, \hat{\theta}_N$ on S^1. We numerically integrated (1.6) for various type I and type II responses and noise strengths. As pulse P, we considered wrapped normal distributions with zero mean and a variance σ_p^2 between 10^{-2} and 10^{-4}. The number of oscillators N ranged from 10^2 to 10^4. We used an explicit two-step Runge–Kutta scheme of mean square order 3/2, as described in [32,

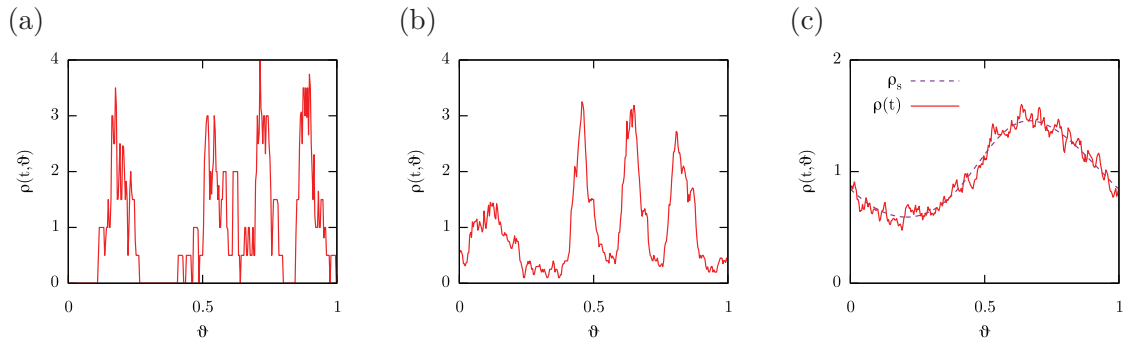

Figure 15. *Example realizations of the integrated Langevin equation* (1.6) *at time* $t = 10^3\ \omega^{-1}$ *for repulsing type* II *responses with* $\vartheta_o = 0.4$. *The illustrated phase densities (solid curve) are estimated using a box kernel density estimator of width* 0.02. *Oscillator count and pulse variance are* (a) $N = 10^2$ *and* $\sigma_\mathrm{p}^2 = 10^{-4}$, (b) $N = 10^3$ *and* $\sigma_\mathrm{p}^2 = 10^{-4}$, *and* (c) $N = 10^4$ *and* $\sigma_\mathrm{p}^2 = 10^{-2}$. *Initial phases were uniformly and independently distributed on* S^1. *For comparison, the stationary state of the Fokker–Planck equation* (1.1) *is plotted with the dashed curve in* (c). *The splitting of the network into four clusters persisted for the lifetime of the simulations in* (a) *and* (b) *(at least up to time* $t = 10^4\ \omega^{-1}$*). The same is true for the seemingly stationary distribution attained in simulation* (c). *The coupling strength is* $|\psi_o|/\omega = 0.5$, *and the noise strength is* $D/\omega = 3 \times 10^{-5}$ *in all cases. The time step used was* $2 \times 10^{-4}\ \omega^{-1}$ *for* (a) *and* (b) *and* 2×10^{-3} *for* (c). *Compare these results to the integration of the corresponding Fokker–Planck equation illustrated in Figure* 13(b).

sect. 3.4, Theorem 3.3]. All random numbers were generated using the libc pseudorandom generator [4]. Normally distributed numbers were generated using the Box–Muller transform [18, sect. 5.2.1]. The time step was set to $\sigma_\mathrm{p}/(50\omega)$; no change in the outcome of the simulations was observed for smaller time steps. Considered parameter values were $\vartheta_o \in \{0.3, 0.4, 0.6, 0.7\}$ (as well as $\vartheta_o = 0.5$ for attracting type II responses) and $|\psi_o|/\omega \in \{0.1, 0.5\}$, $D/\omega \in [0, 0.1]$. The phases $\hat{\theta}_1, \ldots, \hat{\theta}_N$ were initially uniformly and independently distributed.

We compared our simulation results to the long term dynamics suggested by the Fokker–Planck equation (1.1), particularly for large N and small pulse variances σ_p^2. Both the Langevin and Fokker–Planck equations were integrated until the network settled on an attractor. The underlying oscillator phase distribution was estimated from the realizations $\hat{\theta}_1, \ldots, \hat{\theta}_N$ using a kernel density estimator [44], based on a box kernel of width 0.02. Preliminary tests revealed a good agreement between the qualitative long term network behavior suggested by the two methods, provided N was large enough (typically above 500) and σ_p^2 small enough (typically below 10^{-4}). Figure 15 illustrates this for a specific repulsing type II response and noise strength by displaying the estimated phase densities after an integration of the Langevin equation for various oscillator counts N and pulse variances σ_p^2. Figure 13(b) shows a simulation of the Fokker–Planck equation for the same response function and noise, where the network eventually settles on its main attractor. The latter is characterized by a splitting into four oscillator groups that are approximately equally sized and approximately synchronized. As can be seen in Figures 15(a) and (b), for sufficiently small pulse widths the network indeed settles on an attractor similar to the main attractor predicted by the Fokker–Planck equation. In fact, this is even true for oscillator counts as "low" as $N = 100$. However, as shown in Figure 15(c) for an even higher oscillator count ($N = 10^4$), an increased pulse

width can lead to a totally different qualitative behavior, in this case an eventual stationarity of the oscillator phase distribution.

8. Conclusion. We have studied a generalized Fokker–Planck equation as an approximation of the dynamics of large pulse-coupled oscillator networks, for which the pulses can be approximated by a Dirac distribution. For networks with the response functions examined in this article, stationarity is locally and apparently also globally stable provided that noise is sufficiently strong. The noise threshold was found to be quite low compared to the intrinsic oscillator dynamics (i.e., $D/\omega \ll 1$). Such behavior has already been observed in the monofrequent Kuramoto model, where the stationary state (usually referred to as the *incoherent state*) is globally stable if and only if the noise exceeds a certain positive threshold D_c (for a fixed frequency and coupling strength) [47, sect. 3.4(a)]. Due to the rotational symmetry of the Kuramoto model, which is nonpresent in our model, the incoherent state is in fact a uniform phase distribution. Similar noise-induced stabilization effects of stationary states and cancelling of oscillations have also been discovered recently in large-scale stochastic networks of firing rate neurons with sigmoidal interactions [49, 50]. In our model, the stationary network activity itself was found to depend nonlinearly on the noise strength for certain response functions, even reaching an extremum at a finite nontrivial noise level.

As noise is reduced, for all but a few critical response parameters, a stable limit cycle emerges from stationarity, on which the network splits up into one or more groups of approximately synchronized oscillators. From a macroscopical point of view, this leads the network activity to oscillate at frequencies often much higher than the intrinsic oscillator frequency. This so-called *main attractor* dominates the dynamics of the network, at least when starting in the proximity of stationarity or uniform phase distributions. Our results thus show that quite simple response function shapes can lead to the emergence of high frequency oscillatory network behavior. These effects may need to be taken into consideration when attempting to fit biophysical neuron models to observed oscillatory activity of neural potential fields. Furthermore, the bifurcation of the main attractor from stationarity and its relation to the eigenperturbations show the importance of stationary states in large networks of short-pulse-coupled oscillators with noise. In the monofrequent Kuramoto model, the unique periodic solution branching from the incoherent state as noise is reduced was shown to be linearly stable and to correspond to a rotating unimodal distribution, interpreted as a partial network synchronization (*coherence*) [47, 2, 8].

For certain attracting type II responses and sufficiently weak noise, a second stable limit cycle was found on which all oscillators are approximately synchronized. This attractor appears at a lower noise level than the main attractor, so that certain hysteresis phenomena are to be expected during slow changes of the system's noise strength. The existence of this attractor is consistent with our recent findings for similar, noise-free networks with short smooth pulses P (i.e., described by (1.2) with $D = 0$) [29]. They show the local stability of the synchronized state for a large class of response functions, including attracting type II ones.

It has recently been shown for the monofrequent Kuramoto model that the system has a one- or two-dimensional global attractor, depending on the noise strength. For noise not less than D_c, that attractor is in fact the incoherent state. For noise less than D_c, it is

homeomorphic to a two-dimensional disk, consisting of orbits connecting incoherence to the periodic solution of partial coherence [19]. This makes the analysis of the long term behavior of the Kuramoto model simpler than that of our model.

Finally, we point out that the comparisons we performed between the Fokker–Planck equation and the finite Winfree model (see section 7) are by no means exhaustive. Nevertheless, they suggest that the Fokker–Planck equation (1.1) studied in this paper is a good starting point for modeling large finite networks of spiking oscillators with noise.

Appendix A. An upper bound for the imaginary part of eigenvalues. Our starting point is the spectral stability analysis of stationarity in noise-free networks, introduced in section 3.1. We show that the eigenvalue equation

$$\chi(\lambda) := 1 - e^{-\lambda T_\mathrm{s}(1)} \left[1 + \omega T_\mathrm{s}(1) \int_0^1 d\varphi \; \rho_\mathrm{s}'(\varphi) e^{\lambda T_\mathrm{s}(\varphi)} \right] = 0$$

(see the proof of Lemma 3.1(1)) cannot be satisfied if $\Re(\lambda) \neq 0$ and

$$|\Im(\lambda)| > \tilde{M} \left[1 - e^{-|\Re(\lambda)| T_\mathrm{s}(1)} \right]^{-1},$$

with $\tilde{M}$ given by

$$\tilde{M} := \frac{1}{T_\mathrm{s}(1)} \left[\frac{2}{\omega} \left| \psi'(0) \right| + \left\| \left(\frac{\psi'}{\mathrm{v_s}} \right)' \right\|_\infty \right]. \tag{A.1}$$

Using $\rho_\mathrm{s}(\varphi) = 1/(T_\mathrm{s}(1)\mathrm{v_s}(\varphi))$, we can write $\chi(\lambda)$ as

$$\chi(\lambda) = 1 - e^{-\lambda T_\mathrm{s}(1)} \left[1 - \frac{1}{T_\mathrm{s}(1)} \int_0^1 d\varphi \; \frac{\psi'(\varphi)}{\mathrm{v_s^2}(\varphi)} e^{\lambda T_\mathrm{s}(\varphi)} \right]. \tag{A.2}$$

We estimate the integral $C := \int_0^1 d\varphi \; \psi'(\varphi) \cdot e^{\lambda T_\mathrm{s}(\varphi)} / \mathrm{v_s^2}(\varphi)$ appearing in (A.2). For $\lambda \neq 0$ we have

$$C = \frac{1}{\lambda} \int_0^1 d\varphi \; \frac{\psi'(\varphi)}{\mathrm{v_s}(\varphi)} \frac{d}{d\varphi} e^{\lambda T_\mathrm{s}(\varphi)} = \frac{1}{\lambda} \frac{\psi'(0)}{\mathrm{v_s}(0)} \left[e^{\lambda T_\mathrm{s}(1)} - 1 \right] - \frac{1}{\lambda} \int_0^1 d\varphi \; e^{\lambda T_\mathrm{s}(\varphi)} \frac{d}{d\varphi} \frac{\psi'(\varphi)}{\mathrm{v_s}(\varphi)}. \tag{A.3}$$

Define $\chi_o(\lambda) := 1 - \chi(\lambda)$ so that

$$|\chi_o(\lambda)| = e^{-\Re(\lambda) T_\mathrm{s}(1)} \left| 1 - C/T_\mathrm{s}(1) \right|. \tag{A.4}$$

Now suppose that $|\Im(\lambda)| > \tilde{M} \left[1 - e^{-|\Re(\lambda)| T_\mathrm{s}(1)} \right]^{-1}$. Consider first the case $\Re(\lambda) < 0$. Then using (A.3) we can estimate

$$|C| \leq \frac{1}{|\Im(\lambda)|} \left[2 \frac{|\psi'(0)|}{\mathrm{v_s}(0)} + \left\| \left(\frac{\psi'}{\mathrm{v_s}} \right)' \right\|_\infty \right] = \frac{\tilde{M} T_\mathrm{s}(1)}{|\Im(\lambda)|}. \tag{A.5}$$

Applying (A.5) to (A.4) yields

$$|\chi_o(\lambda)| \geq e^{-\Re(\lambda) T_\mathrm{s}(1)} \left(1 - |C| / T_\mathrm{s}(1) \right) \geq e^{-\Re(\lambda) T_\mathrm{s}(1)} \cdot \left(1 - \tilde{M} / |\Im(\lambda)| \right) > 1,$$

which is a contradiction to the eigenvalue equation. Now consider the case $\Re(\lambda) > 0$. From (A.3) we can estimate

$$|C| \le \frac{1}{|\Im(\lambda)|}\left[2\frac{|\psi'(0)|}{\mathrm{v_s}(0)} + \left\|\left(\frac{\psi'}{\mathrm{v_s}}\right)'\right\|_\infty\right] e^{\Re(\lambda)T_\mathrm{s}(1)} = \frac{\tilde{M}T_\mathrm{s}(1)}{|\Im(\lambda)|}e^{\Re(\lambda)T_\mathrm{s}(1)}. \tag{A.6}$$

Applying (A.6) to (A.4) yields

$$|\chi_o(\lambda)| \le e^{-\Re(\lambda)T_\mathrm{s}(1)}\left(1 + |C|\,/T_\mathrm{s}(1)\right) \le e^{-\Re(\lambda)T_\mathrm{s}(1)} + \frac{\tilde{M}}{|\Im(\lambda)|} < 1,$$

which again contradicts the eigenvalue equation. ∎

Appendix B. Elaborations on the numerical analysis. We provide technical details of the numerical methods outlined in section 4. They are to be understood in the context of the respective section referring to them.

B.1. Solving the stationary state equations. As a starting point for the fixed-point iteration we took the stimulus value 1, corresponding to the uniform density. The iteration process was ended whenever subsequent iterations changed the stationary stimulus only by a value less than 10^{-3}. Within the considered parameter range the iteration always converged to a limit in $[0, 2]$ independently on the starting value, for starting values within $[0, 1000]$.

B.2. Solving the eigenvalue equation for noise-free networks. For the numerical solution of the eigenvalue equation (3.2), we used Newton's method with quadratic backtracking [39]. Starting values were taken on a sufficiently fine grid covering a domain deemed large enough for our purposes. Specifically, the distance of adjacent grid points was taken to be roughly one tenth of $2\pi/T_\mathrm{s}(1)$, the latter corresponding to the typical distance between successive eigenvalues, as suggested by Lemma 3.1(2). This length scale is also verified analytically for symmetric type I and type II responses in sections 5 and 6, respectively. In order to limit the search to a finite domain, we used the estimate $|\Im(\lambda)| \le \tilde{M}\cdot\left(1 - e^{-|\Re(\lambda)|T_\mathrm{s}(1)}\right)^{-1}$, valid for any eigenvalue $\lambda \in \sigma_\mathrm{p}(\mathcal{Q})$ with $\Re(\lambda) \neq 0$. The constant $\tilde{M}$, given in (A.1), depends on ψ and ω and was calculated numerically. A proof of this estimate is given in Appendix A. In view of this estimate and Lemma 3.1(2), we limited the grid a priori to the domain $[-M, M] + i\mathbb{R}_+$, where $M := \rho_\mathrm{s}(0)\,\|\psi'\|_\infty$. This domain was scanned in a real-part-first and increasing imaginary part direction. As soon as an eigenvalue $\lambda \in \mathbb{C}$ with nontrivial real part was found, the domain's imaginary part was reduced (if applicable) on the corresponding (left or right) half plane in a way that no eigenvalues with real parts of comparable or greater magnitude would be omitted. More precisely, if the search domain was $([-M, 0] + i\cdot[0, N_\mathrm{l})) \cup ([0, M] + i\cdot[0, N_\mathrm{r}))$, then finding a new eigenvalue λ with $\Re(\lambda) < 0$ would reduce it to $([-M, 0] + i\cdot[0, \tilde{N}_\mathrm{l})) \cup ([0, M] + i\cdot[0, N_\mathrm{r}))$, where

$$\tilde{N}_\mathrm{l} := \max\left\{N_\mathrm{min}, \min\left\{N_\mathrm{l}, \tilde{M}\left(1 - e^{-|\Re(\lambda)|T_\mathrm{s}(1)}\right)^{-1} + \omega\right\}\right\}.$$

Similar adjustments were made when $\Re(\lambda) > 0$. The lower limit $N_\mathrm{min} > 0$ was set sufficiently high to get an acceptable picture of the point spectrum at hand (recall that by Lemma 3.1(2) the point spectrum approaches the grid $i2\pi/T_\mathrm{s}(1)\cdot\mathbb{Z}$ for larger imaginary parts). The

number of iterations was limited to 500 per start value. During these iterations, an attained value $\lambda \in \mathbb{C}$ was considered to be an eigenvalue if it satisfied the eigenvalue equation (3.2) up to an error of less than $\omega^{-2}/1000$ and if subsequent iteration values differed only by less than $\omega/100$. Eigenvalues closer than $\omega/100$ to each other were considered identical. Through numerical quadratures for the representation (3.4), we approximated the shapes of eigenperturbations corresponding to the found eigenvalues. Their periodicity (equivalent to the eigenvalue equation) served as a verification of their correctness.

B.3. Solving the eigenvalue equation for noisy networks. The cutoff of higher order parts of the hierarchy (3.9) corresponds to the approximation of the low-order point spectrum of the linear operator $\mathcal{Q}_D : C^2_{\mathrm{zm}}(S^1) \subseteq \mathcal{C}_{\mathrm{zm}}(S^1) \to \mathcal{C}_{\mathrm{zm}}(S^1)$ by the spectrum of the finite matrix $Q^{(N)} \in \mathbb{C}^{2N\times 2N}$, defined as

$$\left(Q^{(N)}\right)_{nk} := -(2\pi n)^2 D\delta_{nk} - i2\pi n\mathcal{F}_{n-k}(\mathrm{v_s}) - i2\pi n\mathcal{F}_n(\psi\rho_{\mathrm{s}}).$$

Here, δ_{nk} is the Kronecker symbol, and the indices n, k range within $I_N := \{-N, \dots, N\} \setminus \{0\}$. The eigenperturbations h were then approximated by the found eigenvectors $(h_n)_{n\in I_N} \in \mathbb{C}^{2N}$ as $h(\vartheta) \approx \sum_{n\in I_N} h_n e^{in2\pi\vartheta}$. The threshold N was chosen to be 100. We used LAPACK [3] for the spectral analysis of $Q^{(N)}$. The Fourier components $\mathcal{F}_n(\mathrm{v_s})$ and $\mathcal{F}_n(\psi\rho_{\mathrm{s}})$ were calculated numerically. Further increasing N did not seem to have any noteworthy influence on the calculated leading eigenvalues or on the approximations of corresponding eigenperturbations.

B.4. Integrating the Fokker–Planck equation. Here we describe the numerical integration scheme used for the Fokker–Planck equation (1.1), based on the spectral method. The idea is to write the density $\rho(t, \vartheta)$ in the spectral form

$$\rho(t, \vartheta) = \sum_{n\in\mathbb{Z}} \rho_n(t) e^{in2\pi\vartheta}. \tag{B.1}$$

Inserting (B.1) into (1.1) yields the hierarchy of differential equations

$$\dot\rho_n(t) + \left[in2\pi\omega + (n2\pi)^2 D\right]\rho_n(t) + i2\pi n \sum_{k\in\mathbb{Z}} \rho_k(t) \sum_{m\in\mathbb{Z}} \mathcal{F}_{n-m}(\psi)\rho_m(t) = 0 \tag{B.2}$$

in the time-dependent Fourier components $(\rho_n)_{n\in\mathbb{Z}}$. We numerically integrated a finite subset of the above hierarchy, ignoring high-order spectral components ρ_n for $|n| > N$, where N is referred to as the *spectral order*. We used an explicit fixed-time-step numerical integration scheme of order 2 in the time step, based on an ad hoc short-time propagator which we derive below. For that, we write the reduced hierarchy as a nonlinear ODE

$$\frac{d\boldsymbol{\rho}(t)}{dt} = -\hat\Omega\boldsymbol{\rho}(t) + S(\boldsymbol{\rho}(t)) \cdot \hat\Psi\boldsymbol{\rho}(t) \tag{B.3}$$

in the vector $\boldsymbol{\rho}(t) := (\rho_n(t))_{|n|\le N} \in \mathbb{C}^{2N+1}$. The matrices $\hat\Omega, \hat\Psi \in \mathbb{C}^{(2N+1)\times(2N+1)}$ are defined as

$$\hat\Omega_{nm} := \left[in2\pi\omega + (n2\pi)^2 D\right]\delta_{nm}, \quad \hat\Psi_{nm} := -in2\pi\mathcal{F}_{n-m}(\psi),$$

with the indices n, m ranging within $\{-N, \dots, N\}$. The *stimulus* $S(\boldsymbol{\rho}(t))$ is defined as

$$S(\boldsymbol{\rho}(t)) := \langle 1, \boldsymbol{\rho}(t)\rangle := \sum_{|n|\le N} \rho_n(t).$$

We note that any solution $\boldsymbol{\rho}(t)$ to (B.3), should it exist, is of class $\mathcal{C}^\infty$. Furthermore, we have

$$\boldsymbol{\rho}(t_o+\delta t) = \exp\left[-\delta t\cdot\hat{\Omega} + R(\delta t, \boldsymbol{\rho}(t_o))\hat{\Psi}\right]\boldsymbol{\rho}(t_o) \tag{B.4}$$

for any start time $t_o \in \mathbb{R}$ and time step $\delta t \ge 0$, where $R(\delta t, \boldsymbol{\rho}(t_o)) := \int_{t_o}^{t_o+\delta t} dt\; S(\boldsymbol{\rho}(t))$. Note that $R(\delta t, \boldsymbol{\rho}(t_o))$ depends on the initial value $\boldsymbol{\rho}(t_o)$ but not on t_o, as the differential equation (B.3) is autonomous. Using the Zassenhaus formula [30] and the fact that $R(\delta t, \boldsymbol{\rho}(t_o)) \in O(\delta t)$ as $\delta t \to 0^+$, we can write (B.4) as

$$\begin{aligned}\boldsymbol{\rho}(t_o+\delta t) &= e^{-\delta t\cdot\hat{\Omega}}\cdot e^{R(\delta t,\boldsymbol{\rho}(t_o))\hat{\Psi}}\cdot\exp\left[\delta t\cdot R(\delta t,\boldsymbol{\rho}(t_o))\cdot\frac{1}{2}[\hat{\Omega},\hat{\Psi}]\right]\boldsymbol{\rho}(t_o)+O(\delta t^3)\\ &= e^{-\delta t\cdot\hat{\Omega}}\left[1+R(\delta t,\boldsymbol{\rho}(t_o))\hat{\Psi}+\frac{1}{2}R^2(\delta t,\boldsymbol{\rho}(t_o))\hat{\Psi}^2\right]\\ &\quad\times\left[1+\delta t\cdot\frac{1}{2}R(\delta t,\boldsymbol{\rho}(t_o))[\hat{\Omega},\hat{\Psi}]\right]\boldsymbol{\rho}(t_o)+O(\delta t^3),\end{aligned} \tag{B.5}$$

with $[\hat{\Omega},\hat{\Psi}] := \hat{\Omega}\hat{\Psi} - \hat{\Psi}\hat{\Omega}$ denoting the commutator of $\hat{\Omega}$ and $\hat{\Psi}$. Note that

$$R(\delta t, \boldsymbol{\rho}(t_o)) = S(\boldsymbol{\rho}(t_o))\delta t + \left.\frac{dS(\boldsymbol{\rho}(\cdot))}{dt}\right|_{t_o}\frac{\delta t^2}{2} + O(\delta t^3), \tag{B.6}$$

where

$$\left.\frac{dS(\boldsymbol{\rho}(\cdot))}{dt}\right|_{t_o} = \sum_{|n|\le N}\left.\frac{d\rho_n}{dt}\right|_{t_o} = \left\langle 1, -\hat{\Omega}\boldsymbol{\rho}(t_o) + \langle 1,\boldsymbol{\rho}(t_o)\rangle\,\hat{\Psi}\boldsymbol{\rho}(t_o)\right\rangle. \tag{B.7}$$

Inserting (B.7) and (B.6) into (B.5) yields $\boldsymbol{\rho}(t_o+\delta t) = \hat{U}_{\mathrm{s}}(\delta t, \boldsymbol{\rho}(t_o)) + O(\delta t^3)$, with the nonlinear *short-time propagator* $\hat{U}_{\mathrm{s}}(\delta t,\ \cdot) : \mathbb{C}^{2N+1} \to \mathbb{C}^{2N+1}$ defined by

$$\begin{aligned}\hat{U}_{\mathrm{s}}(\delta t, \boldsymbol{\rho}(t_o)) :=& e^{-\delta t\cdot\hat{\Omega}}\left[1+R_s(\delta t,\boldsymbol{\rho}(t_o))\hat{\Psi}+\frac{1}{2}R_s^2(\delta t,\boldsymbol{\rho}(t_o))\hat{\Psi}^2\right]\\ &\times\left[1+\delta t\cdot R_s(\delta t,\boldsymbol{\rho}(t_o))\cdot\frac{1}{2}[\hat{\Omega},\hat{\Psi}]\right]\boldsymbol{\rho}(t_o),\\ R_s(\delta t,\boldsymbol{\rho}(t_o)) :=& \langle 1,\boldsymbol{\rho}(t_o)\rangle\,\delta t + \left\langle 1, -\hat{\Omega}\boldsymbol{\rho}(t_o) + \langle 1,\boldsymbol{\rho}(t_o)\rangle\,\hat{\Psi}\boldsymbol{\rho}(t_o)\right\rangle\frac{\delta t^2}{2}.\end{aligned}$$

Setting $\boldsymbol{\rho}^{(0)} := \boldsymbol{\rho}(0)$ as the starting value and defining the step $\boldsymbol{\rho}^{(n+1)} := \hat{U}_s(\delta t, \boldsymbol{\rho}^{(n)})$, we obtain an explicit fixed-time-step numerical integration scheme for (B.3) of order 2 in δt, with $\boldsymbol{\rho}^{(n)}$ approximating $\boldsymbol{\rho}(n\cdot\delta t)$. The technique follows the ideas of the well-known Feynman path integral method for the Schrödinger equation [16, 43, 51].

The spectral order N was chosen large enough for $\sum_{|n|\leq N/2}\rho_n(0)e^{in2\pi\cdot(\cdot)}$ and $\sum_{|n|\leq N/2}\mathcal{F}_n(\psi)e^{in2\pi\cdot(\cdot)}$ to adequately represent the initial density $\rho(0,\cdot)$ and response function $\psi(\cdot)$, respectively. Typical values were $N\gtrsim 100$; further increases in N did not seem to have any notable effects. We mention that in the case $D>0$, explicit fixed-time-step Runge–Kutta methods for (B.3) of order up to 4 turned out to be less efficient, requiring impractically small time steps to ensure satisfactory accuracy. This stiffness of the system [11, sect. 5.11] can be traced back to the factor n^2D dominating the differential equation (B.2) for larger orders n. Typical time steps ranged between 2×10^{-4} and 2×10^{-5}. The integration was aborted when the modulus of the marginal components $\rho_{\pm N}$ exceeded 10^{-4}. This was the case whenever narrow peaks appeared in the distribution $\rho(t,\cdot)$ and in fact was encountered only for low noise strengths ($D/\omega\lesssim10^{-5}$).

Appendix C. The point spectrum for symmetric type I responses. For noise-free networks with symmetric type I responses $\psi(\vartheta)=\frac{\psi_o}{2}[1-\cos(2\pi\vartheta)]$, we provide an analytical treatment of the eigenvalue equation (3.2) for the linearized dynamics at the stationary state ρ_{s}. We assume $\psi_o\neq0$, since otherwise the point spectrum is easily found to be given by (5.2). The corresponding stationary stimulus $\rho_{\mathrm{s}}(0)$ is given by (5.1). The eigenvalue equation takes the form

$$\int_0^1 \frac{d\vartheta\; e^{\lambda T_{\mathrm{s}}(\vartheta)}}{\left[\omega+\frac{\psi_o}{2}\rho_{\mathrm{s}}(0)\,[1-\cos(2\pi\vartheta)]\right]^2}=0, \tag{C.1}$$

with the travel time $T_{\mathrm{s}}(\vartheta)$ introduced in Lemma 3.1 for $\vartheta\in[0,1]$ given by

$$T_{\mathrm{s}}(\vartheta)=\frac{1}{\pi\omega\sqrt{1+\frac{\psi_o}{\omega}\rho_{\mathrm{s}}(0)}}\cdot\arctan\left[\sqrt{1+\frac{\psi_o}{\omega}\rho_{\mathrm{s}}(0)}\cdot\tan(\pi\vartheta)\right].$$

Note that $\arctan(\cdot)$ is evaluated so that $T_{\mathrm{s}}(0)=0$ and $T_{\mathrm{s}}(\vartheta)$ is continuous in $\vartheta\in[0,1]$. The left-hand side of (C.1) evaluates to

$$\frac{Q(\lambda)}{4\omega\lambda}\cdot\frac{e^{\lambda/(\rho_{\mathrm{s}}(0)\omega)}-1}{\lambda^2+2\pi^2\psi_o\rho_{\mathrm{s}}(0)\omega+(2\pi\omega)^2},$$

with

$$Q(\lambda):=(2\lambda)^2+2\psi_o\rho_{\mathrm{s}}(0)\omega(2\pi)^2+(4\pi\omega)^2,$$

provided that $\lambda\neq0$ and $\lambda^2+2\pi^2\psi_o\rho_{\mathrm{s}}(0)\omega+(2\pi\omega)^2\neq0$, that is, $\lambda\notin\{0,\pm i2\pi\omega\rho_{\mathrm{s}}(0)\}$. Clearly, $\lambda=0$ does not satisfy the eigenvalue equation (C.1). It is easy to see that

$$\lim_{\lambda\to\pm i2\pi\omega\rho_{\mathrm{s}}(0)}\frac{e^{\lambda/(\rho_{\mathrm{s}}(0)\omega)}-1}{\lambda^2+2\pi^2\psi_o\rho_{\mathrm{s}}(0)\omega+(2\pi\omega)^2}=\mp\frac{1}{\rho_{\mathrm{s}}(0)^2\omega^2}\cdot\frac{i}{4\pi}.$$

Consequently, the left-hand side of (C.1) tends with $\lambda\to\pm i2\pi\omega\rho_{\mathrm{s}}(0)$ to

$$-\frac{Q(\pm i2\pi\omega\rho_{\mathrm{s}}(0))}{4\omega\cdot i2\pi\omega\rho_{\mathrm{s}}(0)}\cdot\frac{1}{\rho_{\mathrm{s}}(0)^2\omega^2}\cdot\frac{i}{4\pi},$$

which is nonzero if $\psi_o \neq 0$. Since the left-hand side of the eigenvalue equation (C.1) is continuous in λ, we conclude that $\pm i2\pi\omega\rho_{\mathrm{s}}(0)$ are not eigenvalues of $\mathcal{Q}$. Consequently, the point spectrum $\sigma_{\mathrm{p}}(\mathcal{Q})$ is given by the solutions of

$$Q(\lambda) \cdot \left[e^{\lambda/(\rho_{\mathrm{s}}(0)\omega)} - 1\right] = 0$$

other than $\{0, \pm i2\pi\omega\rho_{\mathrm{s}}(0)\}$. We thus arrive at (5.2).

Appendix D. The point spectrum for symmetric type II responses. We consider noise-free networks with symmetric type II responses $\psi(\vartheta) = -\psi_0 \sin(2\pi\vartheta)$. We present an analytical evaluation of the eigenvalue equation (3.2). We assume $\psi_o \neq 0$, since otherwise the point spectrum is easily found by (6.2). The corresponding stationary stimulus $\rho_{\mathrm{s}}(0)$ is given by (6.1). The eigenvalue equation takes the form

$$\int_0^1 \frac{d\vartheta\ e^{\lambda T_{\mathrm{s}}(\vartheta)}}{\left[\omega - \psi_o\rho_{\mathrm{s}}(0)\sin(2\pi\vartheta)\right]^2} = 0. \tag{D.1}$$

The travel time $T_{\mathrm{s}}(\vartheta)$ introduced in Lemma 3.1 is for $\vartheta \in [0,1]$ given by

$$T_{\mathrm{s}}(\vartheta) = -\frac{1}{\pi\omega\sqrt{1-(\psi_o\rho_{\mathrm{s}}(0)/\omega)^2}} \cdot \arctan\left[\frac{\psi_o\rho_{\mathrm{s}}(0) - \omega\tan(\pi\vartheta)}{\sqrt{\omega^2 - \psi_o^2\rho_{\mathrm{s}}^2(0)}}\right] + C_{\mathrm{s}},$$

with the constant C_{s} chosen and $\arctan(\cdot)$ evaluated so that $T_{\mathrm{s}}(0) = 0$ and $T_{\mathrm{s}}(\vartheta)$ is continuous in $\vartheta \in [0,1]$. The left-hand side of (D.1) evaluates to

$$\frac{1}{\lambda\omega} \cdot \frac{\lambda^2 + (2\pi\omega)^2 - 2\pi\psi_o\rho_{\mathrm{s}}(0)\lambda}{\lambda^2 + (2\pi)^2(\omega^2 - \psi_o^2\rho_{\mathrm{s}}^2(0))} \cdot \left[e^{\lambda/(\rho_{\mathrm{s}}(0)\omega)} - 1\right], \tag{D.2}$$

provided that $\lambda^2 + (2\pi)^2(\omega^2 - \psi_o^2\rho_{\mathrm{s}}^2(0)) \neq 0$ and $\lambda \neq 0$, that is, $\lambda \notin \{0, \pm 2\pi i/T_{\mathrm{s}}(1)\}$. Here we used the fact that $T_{\mathrm{s}}(1) = 1/(\rho_{\mathrm{s}}(0)\omega)$. It is easy to see that

$$\lim_{\lambda \to \pm(2\pi i\rho_{\mathrm{s}}(0)\omega)} \frac{e^{\lambda/(\rho_{\mathrm{s}}(0)\omega)} - 1}{\lambda^2 + (2\pi)^2(\omega^2 - \psi_o^2\rho_{\mathrm{s}}^2(0))} = \mp\frac{1}{\omega^2\rho_{\mathrm{s}}^2(0)} \cdot \frac{i}{4\pi}. \tag{D.3}$$

Applying (D.3) to the representation (D.2), we find that the left-hand side of (D.1) tends to

$$-\frac{1}{2\pi i\rho_{\mathrm{s}}(0)\omega} \cdot \frac{1}{\omega^2\rho_{\mathrm{s}}^2(0)} \cdot \frac{i}{4\pi} \cdot \frac{\psi_o\omega(2\pi)^2(\psi_o \mp i\omega)}{\omega^2 + \psi_o^2} \neq 0$$

as $\lambda \to \pm 2\pi i/T_{\mathrm{s}}(1)$. By continuity in λ, we conclude that $\{\pm 2\pi i/T_{\mathrm{s}}(1)\}$ are not eigenvalues of $\mathcal{Q}$. Clearly, $\lambda = 0$ does not solve (D.1). Thus, the eigenvalues of $\mathcal{Q}$ are the solutions of

$$\left[\lambda^2 + (2\pi\omega)^2 - 2\pi\psi_o\rho_{\mathrm{s}}(0)\lambda\right] \cdot \left[e^{\lambda/(\rho_{\mathrm{s}}(0)\omega)} - 1\right] = 0 \tag{D.4}$$

other than $\{0, \pm 2\pi i/T_{\mathrm{s}}(1)\}$. Solving (D.4) finally yields the point spectrum (6.2).

Acknowledgments. This work was conducted with the support of the Max Planck Institute for Mathematics in the Sciences, Leipzig, Germany. We thank our two reviewers for their valuable comments and suggestions.

REFERENCES

[1] L. F. Abbott and C. van Vreeswijk, *Asynchronous states in networks of pulse-coupled oscillators*, Phys. Rev. E, 48 (1993), pp. 1483–1490.

[2] J. A. Acebrón, L. L. Bonilla, C. J. P. Vicente, F. Ritort, and R. Spigler, *The Kuramoto model: A simple paradigm for synchronization phenomena*, Rev. Modern Phys., 77 (2005), pp. 137–185.

[3] E. Anderson, Z. Bai, C. Bischof, S. Blackford, J. Demmel, J. Dongarra, J. Du Croz, A. Greenbaum, S. Hammarling, A. McKenney, and D. Sorensen, *LAPACK Users' Guide*, 3rd ed., SIAM, Philadelphia, 1999.

[4] Apple Inc., *Random, part of bsd libc*, Standard C Library, Darwin 10.8.0, Apple, Cupertino, CA, 2011.

[5] J. T. Ariaratnam, *Collective Dynamics of the Winfree Model of Coupled Nonlinear Oscillators*, Ph.D. thesis, Cornell University, Ithaca, NY, 2002.

[6] J. T. Ariaratnam and S. H. Strogatz, *Phase diagram for the Winfree model of coupled nonlinear oscillators*, Phys. Rev. Lett., 86 (2001), pp. 4278–4281.

[7] L. Basnarkov and V. Urumov, *Critical exponents of the transition from incoherence to partial oscillation death in the Winfree model*, J. Stat. Mech., 2009 (2009), P10014.

[8] L. Bertini, G. Giacomin, and K. Pakdaman, *Dynamical aspects of mean field plane rotators and the Kuramoto model*, J. Stat. Phys., 138 (2010), pp. 270–290.

[9] L. L. Bonilla, *Stable nonequilibrium probability densities and phase transitions for meanfield models in the thermodynamic limit*, J. Stat. Phys., 46 (1987), pp. 659–678.

[10] L. L. Bonilla, J. C. Neu, and R. Spigler, *Nonlinear stability of incoherence and collective synchronization in a population of coupled oscillators*, J. Stat. Phys., 67 (1992), pp. 313–330.

[11] R. L. Burden and J. D. Faires, *Numerical Analysis*, 7th ed., Brooks Cole, Independence, KY, 2001.

[12] J. D. Crawford and K. T. R. Davies, *Synchronization of globally coupled phase oscillators: Singularities and scaling for general couplings*, Phys. D, 125 (1999), pp. 1–46.

[13] D. A. Dawson, *Critical dynamics and fluctuations for a mean-field model of cooperative behavior*, J. Stat. Phys., 31 (1983), pp. 29–85.

[14] D. Desmaisons, J. D. Vincent, and P. M. Lledo, *Control of action potential timing by intrinsic subthreshold oscillations in olfactory bulb output neurons*, J. Neurosci., 19 (1999), pp. 10727–10737.

[15] G. B. Ermentrout, *Type* I *membranes, phase resetting curves, and synchrony*, Neural Comput., 8 (1996), pp. 979–1001.

[16] R. P. Feynman and A. R. Hibbs, *Quantum Mechanics and Path Integrals*, Internat. Ser. Pure Appl. Phys., McGraw–Hill, New York, 1965.

[17] T. D. Frank, *Nonlinear Fokker-Planck Equations: Fundamentals and Applications*, Springer, New York, 2005.

[18] J. E. Gentle, *Random Number Generation and Monte Carlo Methods*, 2nd ed., Statistics and Computing, Springer, New York, 2003.

[19] G. Giacomin, K. Pakdaman, and X. Pellegrin, *Global attractor and asymptotic dynamics in the Kuramoto model for coupled noisy phase oscillators*, Nonlinearity, 25 (2012), pp. 1247–1273.

[20] F. Giannuzzi, D. Marinazzo, G. Nardulli, M. Pellicoro, and S. Stramaglia, *Phase diagram of a generalized Winfree model*, Phys. Rev. E, 75 (2007), 051104.

[21] P. Goel and B. Ermentrout, *Synchrony, stability, and firing patterns in pulse-coupled oscillators*, Phys. D, 163 (2002), pp. 191–216.

[22] D. Hansel, G. Mato, and C. Meunier, *Synchrony in excitatory neural networks*, Neural Comput., 7 (1995), pp. 307–337.

[23] E. J. Hildebrand, M. A. Buice, and C. C. Chow, *Kinetic theory of coupled oscillators*, Phys. Rev. Lett., 98 (2007), 054101.

[24] H. B. Hollinger, *Molecular chaos and the Boltzmann equation*, J. Chem. Phys., 36 (1962), 3208.

[25] Y. Kuramoto, *Self-entrainment of a population of coupled non-linear oscillators*, in International Symposium on Mathematical Problems in Theoretical Physics, Lecture Notes in Phys. 39, Springer, Berlin, 1975, pp. 420–422.

[26] Y. Kuramoto and H. Arakai, *Chemical Oscillations, Waves and Turbulence*, Springer, New York, 1984.

[27] S. Lagier, A. Carleton, and P. M. Lledo, *Interplay between local GABAergic interneurons and relay neurons generates γ oscillations in the rat olfactory bulb*, J. Neurosci., 24 (2004), pp. 4382–4392.
[28] R. E. Langer, *On the zeros of exponential sums and integrals*, Bull. Amer. Math. Soc., 37 (1931), pp. 213–239.
[29] S. Louca and F. M. Atay, *Spatially structured networks of pulse-coupled phase oscillators on metric spaces*, submitted.
[30] W. Magnus, *On the exponential solution of differential equations for a linear operator*, Comm. Pure Appl. Math., 7 (1954), pp. 649–673.
[31] K. V. Mardia and P. E. Jupp, *Directional Statistics*, Wiley Series in Probability and Statistics, Wiley, Chichester, UK, 2000.
[32] G. N. Milstein, *Numerical Integration of Stochastic Differential Equations*, Math. Appl. 313, Kluwer, Dordrecht, The Netherlands, 1995.
[33] T. I. Netoff, C. D. Acker, J. C. Bettencourt, and J. A. White, *Beyond two-cell networks: Experimental measurement of neuronal responses to multiple synaptic inputs*, J. Comput. Neurosci., 18 (2005), pp. 287–295.
[34] K. Ota, T. Omori, S. Watanabe, H. Miyakawa, M. Okada, and T. Aonishi, *Measurement of infinitesimal phase response curves from noisy real neurons*, Phys. Rev. E, 84 (2011), 041902.
[35] E. Ott and T. M. Antonsen, *Low dimensional behavior of large systems of globally coupled oscillators*, Chaos, 18 (2008), 037113.
[36] C. J. Perez and F. Ritort, *A moment-based approach to the dynamical solution of the Kuramoto model*, J. Phys. A, 30 (1997), pp. 8095–8103.
[37] A. Pikovsky and S. Ruffo, *Finite-size effects in a population of interacting oscillators*, Phys. Rev. E, 59 (1999), pp. 1633–1636.
[38] G. Pólya, *Über die Nullstellen gewisser ganzer Funktionen*, Math. Z., 2 (1918), pp. 352–383.
[39] W. H. Press, S. A. Teukolsky, W. T. Vetterling, and B. P. Flannery, *Numerical Recipes in C: The Art of Scientific Computing*, Cambridge University Press, Cambridge, UK, 1997.
[40] A. J. Preyer and R. J. Butera, *Neuronal oscillators in Aplysia californica that demonstrate weak coupling in vitro*, Phys. Rev. Lett., 95 (2005), 138103.
[41] H. Risken, *The Fokker-Planck Equation: Methods of Solution and Applications*, 2nd ed., Springer Ser. Synergetics 18, Springer, Berlin, 1989.
[42] H. Sakaguchi, *Cooperative phenomena in coupled oscillator systems under external fields*, Progr. Theoret. Phys., 79 (1988), pp. 39–46.
[43] L. S. Schulman, *Techniques and Applications of Path Integration*, John Wiley and Sons, New York, 1981.
[44] B. W. Silverman, *Density Estimation for Statistics and Data Analysis*, Monographs on Statistics and Applied Probability, Chapman and Hall, London, 1986.
[45] R. M. Smeal, G. B. Ermentrout, and J. A. White, *Phase-response curves and synchronized neural networks*, Philos. Trans. Roy. Soc. B, 365 (2010), pp. 2407–2422.
[46] S. H. Strogatz, *From Kuramoto to Crawford: Exploring the onset of synchronization in populations of coupled oscillators*, Phys. D, 143 (2000), pp. 1–20.
[47] S. H. Strogatz and R. E. Mirollo, *Stability of incoherence in a population of coupled oscillators*, J. Stat. Phys., 63 (1991), pp. 613–635.
[48] J. Touboul, *Propagation of Chaos in Neural Fields*, preprint, arXiv:1108.2414, 2011.
[49] J. Touboul, *Mean-field equations for stochastic firing-rate neural fields with delays: Derivation and noise-induced transitions*, Phys. D, 241 (2012), pp. 1223–1244.
[50] J. Touboul, G. Hermann, and O. Faugeras, *Noise-induced behaviors in neural mean field dynamics*, SIAM J. Appl. Dyn. Syst., 11 (2012), pp. 49–81.
[51] M. F. Wehner and W. G. Wolfer, *Numerical evaluation of path-integral solutions to Fokker-Planck equations*, Phys. Rev. A, 27 (1983), pp. 2663–2670.
[52] A. T. Winfree, *Biological rhythms and the behavior of populations of coupled oscillators*, J. Theoret. Biol., 16 (1967), pp. 15–42.